The evolution of immiscible silicate and fluoride melts: Implications for REE ore-genesis

O. Vasyukova and A.E. Williams-Jones

Department of Earth and Planetary Sciences, McGill University, 3450 University Street Montreal, Quebec, Canada, H3A 0E8, olga.vasyukova@mcgill.ca

Abstract

The Mid-Proterozoic peralkaline Strange Lake pluton (Québec-Labrador, Canada) exhibits extreme enrichment in high field strength elements (HFSE), including the rare earth elements (REE), particularly in pegmatites. On the basis of a study of melt inclusions, we proposed recently that fluoride-silicate melt immiscibility played an important and perhaps dominant role in concentrating the REE within the pluton. Here we present further evidence for silicate-fluoride immiscibility at Strange Lake from a sample of the hypersolvus granite, which contains an inclusion composed largely of REE and HFSE minerals.

The inclusion (~5 cm in diameter) comprises a narrow rim containing chevkinite-(Ce) and zircon in a fluorite matrix, a core of fluorbritholite-(Ce) and bastnäsite-(Ce) and a transition zone between the rim and the core consisting of a fine-grained intergrowth of bastnäsite-(Ce), gagarinite-(Y) and fluorite. We propose that the inclusion formed as a result of silicate-fluoride immiscibility, which occurred early in the emplacement history of the Strange Lake pluton, and that it represents the fluoride melt. After separation of the two melts, the boundary between them acted as a locus of crystallisation, where crystals formed repeatedly due to heterogeneous (surface catalysed) nucleation. Zircon crystallised shortly after melt phase separation, and was

Vasyukova, O.V., Williams-Jones, A.E., 2016. The evolution of immiscible silicate and fluoride melts: implications for REE ore-genesis. Geochimica et Cosmochimica Acta 172, 205-224. DOI:10.1016/j.gca.2015.09.018

followed by the growth of perthite together with arfvedsonite and quartz. As a result, the silicate melt surrounding the fluoride inclusion became enriched in volatiles that facilitated crystallisation of progressively larger crystals in the inclusion; large crystals of arfvedsonite and perthite were succeeded by even larger crystals of quartz. Massive crystallisation of chevkinite-(Ce) followed, forming the rim of the inclusion. The fluoride melt, which constituted the matrix to the silicate minerals and chevkinite-(Ce), crystallised after chevkinite-(Ce), forming fluorbritholite-(Ce) and fluorite.

Aqueous fluid exsolved from the silicate melt and altered the inclusion, replacing fluorbritholite-(Ce) with fluocerite-(Ce) and then bastnäsite-(Ce). This was followed by the formation of a fine-grained intergrowth of bastnäsite-(Ce), gagarinite-(Y) and fluorite at the expense of the earlier bastnäsite-(Ce). Chevkinite-(Ce) was not affected. Zircon, however, was replaced by anhydrous zirconosilicates and, in turn, by hydrous zirconosilicates.

The inclusion represents the first macroscopic example of silicate-fluoride immiscibility in nature. We propose that globules of the fluoride melt were initially dispersed within the silicate melt and preserved only rarely in unaltered hypersolvus granite. They accumulated in the residual melt (and therefore in pegmatites) scavenging REE, Ca and F from the silicate melt and, with rare exceptions, were later destroyed by fluids. The latter process contributed significantly to the enrichment of the host rocks in REE, Ca and F.

Introduction

Although fluoride-silicate melt immiscibility has been demonstrated experimentally, (e.g.,Veksler et al., 2005), there have been only three reported occurrences of this phenomenon in nature. Vasyukova and Williams-Jones (Vasyukova and Williams-Jones, 2014) reported the

Vasyukova, O.V., Williams-Jones, A.E., 2016. The evolution of immiscible silicate and fluoride melts: implications for REE ore-genesis. Geochimica et Cosmochimica Acta 172, 205-224. DOI:10.1016/j.gca.2015.09.018

occurrence of fluoride-silicate immiscibility on the basis of observations of quartz-hosted micron-scale melt inclusions in the peralkaline Strange Lake granites, Northern Québec, Canada; the other occurrences were reported by Klemme (2004) and Peretyazhko et al. (2007). The inclusions described by Vasyukova and Williams-Jones (Vasyukova and Williams-Jones, 2014) were found in the earliest, unaltered granite (hypersolvus granite) and were completely crystallised. After heating to 900-950 °C and subsequent quenching, however, some of the silicate melt inclusions were observed to contain a fluoride glass (or in some cases two separate fluoride glasses). This indicated that the inclusions had trapped immiscible silicate and fluoride melts, and that melt immiscibility occurred early in the crystallisation history of the pluton. Most significantly, the fluoride glasses were preferentially enriched in the REE and the silicate glass in Zr, consistent with the experimental findings of Veksler et al. (2005; 2012) that the REE partition strongly into the fluoride melt, and Zr generally favours the silicate melt. Based on these observations, Vasyukova and Williams-Jones (Vasyukova and Williams-Jones, 2014) proposed that the fluoride melts scavenged REE, Ca and F from the silicate melt, that they concentrated the REE in the late-forming pegmatites, and that they served as a source for these elements during hydrothermal remobilisation.

The current study deals with a large inclusion (~5 cm in diameter) that was found in the early, least evolved, hypersolvus granite, and contains approximately 50 vol.% REE minerals. As we will show in this paper, the inclusion provides the first macroscopic evidence of silicate-fluoride melt immiscibility in nature, and offers a unique opportunity to investigate the processes that govern the evolution of immiscible silicate and fluoride melts. Unlike the melt inclusions in quartz that were described in Vasyukova and Williams-Jones (2014), and which preserved information about a relatively late stage of magma evolution (quartz was one of the last phases to

Vasyukova, O.V., Williams-Jones, A.E., 2016. The evolution of immiscible silicate and fluoride melts: implications for REE ore-genesis. Geochimica et Cosmochimica Acta 172, 205-224. DOI:10.1016/j.gca.2015.09.018

crystallise in the hypersolvus granite), the inclusion described here potentially preserves information about the earlier stages of emplacement of the Strange Lake pluton. As the inclusion was not encapsulated in a crystal, it was subjected to alteration and therefore also contains information about the later hydrothermal stages of the evolution of the pluton. As a result, this inclusion permitted a comprehensive reconstruction of the history of the pluton starting from the moment of separation of the fluoride melt from the silicate melt, through the crystallisation of primary minerals, to the hydrothermal alteration and formation of secondary phases.

Geological setting

The peralkaline Strange Lake granite (1240 ± 2 Ma; (Miller et al., 1997)) was emplaced along the contact between Elsonian (1500-1400 Ma) quartz monzonites and paragneisses of Hudsonian (1750-1800 Ma) age, and comprises three granite facies and pegmatites (Fig. 1). The earliest of these granites, the hypersolvus granite occupies the central to southeastern part of the pluton and is distinguished from the later subsolvus facies by the presence of perthite and absence of primary albite (Boily and Williams-Jones, 1994). The hypersolvus granite is equigranular and medium-grained, and contains anhedral quartz and arfvedsonite in interstices between euhedral to subhedral feldspar crystals. Subsolvus granite is volumetrically the most important of the granite facies and occupies the outer part of the massif. It is equigranular and contains primary microcline and albite crystals. The interval between the hypersolvus and subsolvus granites is occupied by transsolvus granite, which contains perthite as phenocrysts and primary albite and microcline in the matrix. There are two main pegmatite fields, one in the north-eastern part of the complex and the other in the centre. Both of them consist of sub-

Vasyukova, O.V., Williams-Jones, A.E., 2016. The evolution of immiscible silicate and fluoride melts: implications for REE ore-genesis. Geochimica et Cosmochimica Acta 172, 205-224. DOI:10.1016/j.gca.2015.09.018

horizontal lenses and sheets ranging in thickness from tens of cm up to 20 m, and both are hosted by altered subsolvus granite.

The pluton has been the target of exploration as it contains high concentrations of the rare earth elements and other high field strength elements in and around pegmatites in the most altered subsolvus granite. Current exploration is centred on the north-eastern pegmatite field, which is referred to as the B-Zone; the central pegmatite field was explored in the early 1980s and is referred to as the Main Zone (Fig. 1). The pegmatites and subsolvus granite in both zones contain high proportions of rare metal minerals, e.g., allanite-(Ce), armstrongite, bastnäsite-(Ce), elpidite, fluocerite-(Ce), gadolinite-(Y), gagarinite-(Y), kainosite-(Y), monazite-(Ce), pyrochlore, titanite and zircon. Smaller proportions of many of these minerals are also present in the hypersolvus and transsolvus granites. An indicated mineral resource of 278 Mt of ore grading, 0.94 wt.% total rare earth oxides (TREO), of which 38% are heavy rare earth oxides (HREO), 1.92 wt.% ZrO_2 and 0.18 wt.% Nb_2O_5 has been delineated in the B-Zone (www.questrareminerals.com).

Methods

Imaging and semi-quantitative mineral identification were carried out using a Hitachi S-3000N VP Scanning Electron Microscope (SEM) equipped with solid state back-scattered electron (BSE) and energy dispersive spectroscopic (EDS) detectors. Selected minerals were analysed quantitatively using a JEOL JXA-8900L electron microprobe equipped with five wavelength dispersive spectrometers (WDS) and a PulseTor Maxim EDS detector. The WDS analyses were conducted at 15 kV, with a 30 nA beam current and a beam diameter of 10 μm for chevkinite-(Ce) and 15 μm for fluorbritholite-(Ce), fluorocarbonates, fluorite and gagarinite-(Y)

Vasyukova, O.V., Williams-Jones, A.E., 2016. The evolution of immiscible silicate and fluoride melts: implications for REE ore-genesis. Geochimica et Cosmochimica Acta 172, 205-224. DOI:10.1016/j.gca.2015.09.018

and 5 μm for zircon. Counting times and detection limits are reported in APPENDIX A. Owing to the small crystal size, it was not possible to use the electron microprobe to quantitatively analyse the zirconosilicates. These minerals were identified from element maps and semi-quantitative EDS analyses using the SEM.

Results

Host granite

The granite hosting the inclusion that is the focus of this study (the inclusion was found in the Alterra Zone, Fig. 1) is typical of the hypersolvus granite unit described by Boily and Williams-Jones (1994). It is pale pink to grey in colour, equigranular and medium-grained; its mineralogy is relatively simple, i.e., it consists mainly of perthite, quartz and arfvedsonite (Fig. 2a). The perthite crystals are large and tabular (0.5-2 mm in length), and occupy about 50-60 vol.% of the rock. They have been hydrothermally altered to albite along their rims. Arfvedsonite is anhedral (0.7-1.5 mm in diameter), fills interstices between perthite crystals, and locally contains inclusions of perthite, fluorite and zircon (Fig. 2a). Commonly, arfvedsonite crystals have been partially altered to astrophyllite ($(K,Na)_3(Fe^{2+},Mn)_7Ti_2Si_8O_{24}(O,OH)_7$), and are spatially associated with a fine-grained intergrowth of zircon, quartz and Na- and K-zirconosilicates, i.e., dalyite ($K_2ZrSi_6O_{15}$) and vlasovite ($Na_2ZrSi_4O_{11}$). Locally, remnants of the intergrowth are embedded in elpidite ($Na_2ZrSi_6O_{15}•3(H_2O)$) (Fig. 2b and c). Unaltered (or slightly altered along their edges) zircon crystals are enclosed in some arfvedsonite crystals (Fig. 2a). The quartz (0.5-1mm) is anhedral and fills interstices between perthite and arfvedsonite crystals.

Vasyukova, O.V., Williams-Jones, A.E., 2016. The evolution of immiscible silicate and fluoride melts: implications for REE ore-genesis. Geochimica et Cosmochimica Acta 172, 205-224. DOI:10.1016/j.gca.2015.09.018

Rare, REE-rich intergrowths are observed within the host granite (Fig. 2b and d). They are composed of fine-grained anhedral bastnäsite-(Ce) ((REE)(CO_3)F) (50-100 μm), fluorite (20-100 μm), quartz (20-70 μm) and euhedral albite (20-70 μm). Locally the quartz contains micro-inclusions of a Y-bearing phase (Fig. 2d).

The inclusion

The inclusion is approximately 5 cm in diameter and roughly ellipsoidal in shape. Macroscopically, it is observed to comprise three distinct zones, a narrow dark-coloured rim (1-2 mm thick), a 5-8 mm thick, light-coloured transition zone and a pale pink-grey core (Fig. 3). Each of the zones is described in detail (mineralogy and textures) below.

Rim zone

The boundary between the host granite and the rim is invariably sharp; locally, major minerals (perthite and quartz) from the surrounding granite protrude into the inclusion, forming mono- or polycrystalline embayments (Fig. 4a). Anhedral arfvedsonite (0.7-1.5 mm in diameter) and, in some cases, aenigmatite ($Na_2Fe^{2+}{}_5Ti(Si_6O_{18})O_2$)), mark the boundary between the host granite and the inclusion (Fig. 4b). The aenigmatite occurs as dark, reddish-brown, unzoned prismatic crystals (up to 1.5 mm in length) aligned along the inclusion border, and locally contains small euhedral zircon crystals as inclusions.

The rim zone may be envisaged as consisting of an assemblage of fluorite, zircon and chevkinite-(Ce) $(La,Ce,Ca)_4(Fe^{2+},Mg)_2(Ti,Fe^{3+})_3Si_4O_{22}$); fluorite constitutes the matrix in which zircon and chevkinite-(Ce) occur. This assemblage crystallised between perthite crystals and fills inclusions and embayments in quartz (Fig. 4c and d). Perthite displays serrated contacts with the other minerals, whereas the boundaries involving quartz are smooth. Arfvedsonite is absent. Albite is commonly found at boundaries between perthite and other minerals.

Vasyukova, O.V., Williams-Jones, A.E., 2016. The evolution of immiscible silicate and fluoride melts: implications for REE ore-genesis. Geochimica et Cosmochimica Acta 172, 205-224. DOI:10.1016/j.gca.2015.09.018

154 The assemblage of fluorite, zircon and chevkinite-(Ce) comprises 30-40% by volume of
155 the rim zone, and locally up to 60 vol.% (Fig. 4a). The volume proportions of fluorite, zircon and
156 chevkinite-(Ce), are approximately 30%, 20% and 50%, respectively. Chevkinite-(Ce), together
157 with the adjacent arfvedsonite and aenigmatite, gives the rim its dark colour.

158 The chevkinite-(Ce) forms stubby reddish brown prismatic crystals (100-200 μm in
159 diameter) and is commonly zoned; the zonation is defined by a subtle variation in REE, Ca, Fe,
160 Ti, Th, Zr and Nb content, which is described in detail below. Locally, chevkinite-(Ce) is partly
161 overgrown on zircon (Fig. 4c, the contact is shown by an arrow).

162 Zircon forms small euhedral crystals (50-150 μm in diameter), which are included in
163 perthite or fluorite (Fig. 4c). Locally, larger anhedral crystals (up to 300 μm in diameter) are
164 observed. Where it is not included in other minerals, zircon has been partially altered to alkali-
165 zirconosilicates, namely, vlasovite, dalyite, catapleiite $(Na,Ca)_2ZrSi_3O_9•2(H_2O)$ and elpidite. The
166 alteration of zircon is the same throughout the inclusion and is similar to that in the host granite;
167 a detailed description is provided later in the section describing alteration within the core.
168 Chevkinite-(Ce) is mostly unaltered; locally it was replaced by karnasurtite-(Ce)
169 $(Ce,La,Th)(Ti,Nb)(Al,Fe^{3+})(Si,P)_2O_7(OH)_4 \cdot 3H_2O$ or in some cases by a fine-grained (5-20 μm)
170 intergrowth of bastnäsite-(Ce), gagarinite-(Y) $(Na(REE_xCa_{1-x})(REE_yCa_{1-y})F_6)$ and fluorite. The
171 intergrowth is most commonly observed in the transition zone, and is described in more detail
172 below. Fluorite also occurs as relatively large (up to 500 μm in diameter) colourless irregularly
173 shaped crystals that enclose zircon and chevkinite-(Ce) (Fig. 4c).

174 **Transition zone**

175 The transition zone has gradational contacts with both the rim and the core (Fig. 5a).
176 Texturally, it is mainly a fine-grained intergrowth of bastnäsite-(Ce), fluorite, gagarinite-(Y) and

Vasyukova, O.V., Williams-Jones, A.E., 2016. The evolution of immiscible silicate and fluoride melts: implications for REE ore-genesis. Geochimica et Cosmochimica Acta 172, 205-224. DOI:10.1016/j.gca.2015.09.018

quartz; the intergrowth is either intermixed with perthite or fills numerous embayments in large quartz crystals (up to 5-7 mm). Albite is commonly found at boundaries between perthite and other minerals. Chevkinite-(Ce) and zircon are present in minor proportions. The REE-rich intergrowth displays interdigitating margins with perthite, and occupies about the same volume proportion as the latter, whereas in contact with quartz it displays smooth margins and the quartz/intergrowth volume ratio is much higher, i.e., approximately 70/30. Locally, the REE-rich intergrowth surrounds other crystals, e.g., chevkinite-(Ce) or zircon. Crystals within the intergrowth are anhedral and do not exceed 50 μm in diameter; commonly the diameter is 5-20 μm (Fig. 5b). This fine-grained intergrowth determines the color of the zone.

Close to the core, relicts of fluorbritholite-(Ce) ($(Ca,Ce,La,Na)_5(SiO_4,PO_4)_3F$) are observed within the intergrowth (Fig. 5c-e). The fluorbritholite-(Ce) is invariably surrounded by bastnäsite-(Ce); remnants of fluorbritholite-(Ce) are rounded or amoeboid in shape and locally were replaced by fluocerite-(Ce) ($REEF_3$) (Fig. 5d) prior to the replacement by bastnäsite-(Ce). The bastnäsite-(Ce) associated with fluorbritholite-(Ce) is different from that described earlier as being part of the fine-grained REE-rich intergrowth. The crystals are significantly larger (50-300 μm), and their appearance is speckled due to the presence of micro-inclusions (Fig. 5d). The composition is also slightly different. To distinguish the two bastnäsite-(Ce) generations, we will refer hereafter to bastnäsite-(Ce) associated with fluorbritholite-(Ce) as bastnäsite-(Ce) R (the R emphasises the fact that it represents remnants) and bastnäsite-(Ce) that is part of the intergrowth mineral assemblage, as bastnäsite-(Ce) I (intergrowth). In some parts of the transition zone, the proportion of speckles within bastnäsite-(Ce) R increases and the speckles become progressively larger and identifiable as fine-grained intergrowths of bastnäsite-(Ce) I, fluorite, quartz and gagarinite-(Y) (Fig. 5c and e). Where the REE intergrowth is in contact with fluorite, the latter

Vasyukova, O.V., Williams-Jones, A.E., 2016. The evolution of immiscible silicate and fluoride melts: implications for REE ore-genesis. Geochimica et Cosmochimica Acta 172, 205-224. DOI:10.1016/j.gca.2015.09.018

occurs as partly resorbed fragments (Fig. 5e shown by the dashed arrow). Anhedral quartz crystals (20-60 μm in diameter) are spatially associated with bastnäsite-(Ce) R and fluorbritholite-(Ce) (Fig. 5c-e).

Chevkinite-(Ce) is significantly less abundant in the transition zone but similar to that in the rim zone, i.e., it is zoned and the zonation is determined by variations in REE, Ca, Fe, Ti, Th, Zr and Nb content. Zircon and fluorite are also less abundant in the transition zone than in the rim, but the zircon crystal morphology and size are similar to those in the rim zone. As in the latter zone, zircon crystals adjacent to boundaries with crystals of other minerals have been partially altered to zirconosilicates.

The core

The core is about 2.5-3 cm in diameter (Fig. 3) and, unlike the transition zone, arfvedsonite is present together with perthite and quartz. As in the transition zone, REE-rich minerals occur together with silicate minerals (mostly perthite, but also arfvedsonite and quartz); the volume ratio of silicate to REE-rich minerals is ~ 40-50/50-60 (Fig. 6a). Perthite crystals are irregular and intermixed with crystals of REE minerals; they display interdigitating margins with arfvedsonite and REE minerals. Arfvedsonite is anhedral (0.5-1.5 mm in diameter) and evenly distributed within the core, but changes its appearance towards the boundary with the transition zone where it becomes much larger (up to 5 mm in diameter, Fig. 3c). These large anhedral crystals of arfvedsonite mark the transition/core boundary. Both types of arfvedsonite are poikilitic and contain numerous inclusions of REE minerals and fluorite; they display smooth boundaries with all minerals, except for perthite, and appear unaltered. Quartz is significantly less abundant than in the transition zone and forms smaller grains (0.3-2 mm in length), but

Vasyukova, O.V., Williams-Jones, A.E., 2016. The evolution of immiscible silicate and fluoride melts: implications for REE ore-genesis. Geochimica et Cosmochimica Acta 172, 205-224. DOI:10.1016/j.gca.2015.09.018

shows the same morphology, i.e., it is anhedral and amoeboid-like with numerous smooth embayments.

In contrast to the transition zone, the REE assemblage in the core does not contain a fine-grained intergrowth of bastnäsite-(Ce) I, gagarinite-(Y) and fluorite but instead comprises fluorbritholite-(Ce), bastnäsite-(Ce) R and fluorite (Fig. 6). The fluorbritholite-(Ce) is almost everywhere replaced by bastnäsite-(Ce) R; unaltered crystals were only observed as inclusions in quartz and arfvedsonite (Fig. 6b and c). Unaltered fluorbritholite-(Ce) crystals are large (50 to 500 μm in diameter) and anhedral (Fig. 6c); their outer surfaces are undulating due to abundant embayments commonly filled with fluorite. No direct contact was observed between perthite and fluorbritholite-(Ce), i.e., bastnäsite-(Ce) R grew at the expense of fluorbritholite-Ce) where it was in contact with perthite. Unlike the contacts between fluorbritholite-(Ce) and arfvedsonite or quartz, those involving bastnäsite-(Ce) R with perthite are interlocked (Fig. 6b). Bastnäsite-(Ce) R in the core is compositionally indistinguishable from bastnäsite-(Ce) R in the transition zone, and also has a speckled appearance due to the presence of micro-inclusions of silicate minerals (Fig. 6b). The proportion of bastnäsite-(Ce) R increases and that of fluorbritholite-(Ce) decreases towards the transition zone. Fluorbritholite-(Ce) and bastnäsite-(Ce) R crystals are spatially associated with fluorite, which occurs as rounded crystals, 50 to 200 μm in diameter, that are enriched in REE in their rims (Fig. 6c). Fluorite contains inclusions of fluorbritholite-(Ce) (Fig. 6c). The proportion of REE-rich minerals relative to fluorite varies significantly, but generally the REE-rich minerals dominate (Fig. 6a).

The chevkinite-(Ce) crystals are similar to those within the rim, but are less common. As is the case for the rim and transition zones, there are two types of zircon crystals in the core, i.e., small, well-shaped unaltered crystals included in feldspar and larger, partly altered interstitial

Vasyukova, O.V., Williams-Jones, A.E., 2016. The evolution of immiscible silicate and fluoride melts: implications for REE ore-genesis. Geochimica et Cosmochimica Acta 172, 205-224. DOI:10.1016/j.gca.2015.09.018

crystals (Fig. 6d). Altered and unaltered zircon crystals, however, may occur in close proximity to each other (Fig. 6d). In backscattered electron images, both varieties of zircon display slightly brighter cores, enriched in Y and other heavy rare earth elements (HREE). The alteration of the zircon is similar to that within the rim and transition zones, i.e., relicts of unaltered zircon are surrounded by zones of a fine-grained intergrowth of zircon, quartz, fluorite, vlasovite, catapleiite and dalyite, which was in turn replaced by elpidite (Fig. 7).

Bulk rock chemistry

The bulk chemical composition of the inclusion, the host granite and the average composition of the hypersolvus Strange Lake granites are reported in Table 1. The hypersolvus granite, which hosts the inclusion, is compositionally similar to hypersolvus granite elsewhere in the Alterra Zone (Fig. 1), except that the rare earth element, calcium and fluorine contents are slightly lower (Table 1). Chondrite-normalised REE profiles of the host granite and the average Alterra hypersolvus granites are very similar (Fig. 8). The profile for the average subsolvus granite is parallel to that of hypersolvus granite but displaced to higher REE content (Fig. 8). By contrast, the chondrite-normalised REE profile for the pegmatites shows HREE-enrichment in Sm, Gd and HREE relative to the subsolvus granite (Fig. 8). All profiles are characterised by relatively strong negative Eu anomalies.

The inclusion is compositionally very different from the host hypersolvus granite (Table 1). Relative to the hypersolvus granite, the inclusion is enriched in the light REE (LREE) (by about two orders of magnitude), highly enriched in Y and the other HREE (by a factor of 20), enriched in F (by an order of magnitude) and Ca (by a factor of five) and depleted in the alkalis and Fe (by a factor of two). The loss on ignition is high (Table 1), consistent with a relatively high proportion of fluorocarbonate minerals. In contrast to the granites, the inclusion is strongly

Vasyukova, O.V., Williams-Jones, A.E., 2016. The evolution of immiscible silicate and fluoride melts: implications for REE ore-genesis. Geochimica et Cosmochimica Acta 172, 205-224. DOI:10.1016/j.gca.2015.09.018

depleted in the HREE relative to the LREE, i.e., the chondrite-normalised REE profile has a steep negative slope (Fig. 8). However, the relative proportions of the REE from La to Gd are very similar to those of the granites, although the absolute concentrations are very much higher. Like those of the granites and pegmatites, the chondrite-normalised REE profile of the inclusion is characterised by a pronounced negative Eu anomaly.

REE mineral and fluorite compositions

Compositional data for the primary REE minerals and fluorite are reported in Table 2 and for the secondary REE minerals in Table 3. The corresponding mineral formulae are reported in Table 4.

On average (76 analyses), the chevkinite-(Ce) contains 47.8±1.3 wt.% total REE oxides, 19.8±0.2 wt.% SiO_2, 16.4±0.7 wt.% TiO_2, 12.2 ±0.4 wt.% total Fe (calculated as FeO), 1.2±0.5 wt.% CaO, 2±0.4 wt.% Nb_2O_5, 0.3±0.2 wt.% ZrO_2 and 0.41±0.06 wt.% F (Table 2). It is strongly enriched in the LREE and depleted in Y and the HREE. The chondrite-normalised REE profile is slightly steeper than that for the bulk inclusion (Fig. 8). As mentioned earlier, the chevkinite-(Ce) is zoned and the zonation is defined by variations in REE, Ca, Fe, Ti, Th, Zr and Nb contents: layers with higher concentrations of Ti, Ca, Zr and Th, have lower REE, Fe and Nb contents (Fig. 9). The average composition of chevkinite-(Ce) is close to that of its end-member, i.e., assuming a total of 22 oxygen atoms per formula unit, the sum of REE and Ca is 3.93 atoms per formula units (apfu), the sum of Fe, Ti, Nb and Zr is 4.95 apfu and the Si content is 4.15 apfu (Table 4).

The fluorbritholite-(Ce) (30 analyses) contains 69.2±1.8 wt.% total REE, 21.6±0.6 wt.% SiO_2, 5.3±1.6 wt.% CaO, 2.8±0.1 wt.% F, 1.5±0.5 wt.% Na_2O and below 1 wt.% Fe (Table 3). It is enriched in the LREE, particularly Pr, Nd and Sm, and has a chondrite-normalised REE

Vasyukova, O.V., Williams-Jones, A.E., 2016. The evolution of immiscible silicate and fluoride melts: implications for REE ore-genesis. Geochimica et Cosmochimica Acta 172, 205-224. DOI:10.1016/j.gca.2015.09.018

291 profile, which is parallel to that for the bulk inclusion, albeit with higher overall REE
292 concentration (Fig. 8). Assuming a total of 13 oxygen atoms per formula unit, the stoichiometric
293 composition of the fluorbritholite-(Ce) corresponds to a sum of REE, Ca and Na of 4.74 apfu, Si
294 of 3 apfu and F of 1.24 apfu (Table 4). The sum of REE is > 3 and Ca < 2; the relatively high Na
295 content reflects a substitution of the type $2Ca^{2+} = REE^{3+} + Na^{+}$.

296 The fluocerite-(Ce) is invariably intergrown with fluorbritholite-(Ce) and/or bastnäsite-
297 (Ce). This precluded precise determination of its composition and stoichiometry. Bastnäsite-(Ce)
298 R (14 analyses) contains 67.7±1.2 wt.% total REE, 21.5±1.9 wt.% CO_2, 7.7±0.8 wt.% F, 3.7±0.5
299 wt.% CaO and 1.7±0.5 wt.% SiO_2 (Table 3). The chondrite-normalised REE profile is almost
300 identical to that of the fluorbritholite-(Ce) (Fig. 8). However, the stoichiometry of the bastnäsite-
301 (Ce) R deviates slightly from the ideal stoichiometry ($REE(CO_2)F$), in that the F content is lower
302 and the SiO_2 content higher. The latter can be attributed to the presence of micro-inclusions of an
303 unknown silicate phase. Assuming a total of 4 oxygen atoms per formula unit, the sum of REE
304 and Ca is 1 apfu, CO_2 is 1.01 and F is 0.83 (Table 4). The deficiency in F can be explained by its
305 substitution by OH; addition of 0.7 wt.% H_2O to the composition of the mineral yields apfu
306 values of 0.99 for REE and Ca, 0.98 for CO_2 and 0.99 for F+OH.

307 Bastnäsite-(Ce) I (26 analyses) contains 74.9±1.3 wt.% total REE, 19.5±0.6 wt.% CO_2,
308 8.4±0.4 wt.% F, and less that a weight percent CaO (Table 3). The chondrite-normalised REE
309 profile is similar to that of bastnäsite-(Ce) R except that bastnäsite-(Ce) I is slightly depleted in
310 Sm and Gd (Fig. 8). Stoichiometrically, bastnäsite-(Ce) I is similar in composition to its end-
311 member ($REE(CO_2)F$), i.e., assuming four oxygen atoms per formula unit, the sum of REE and
312 Ca is 1.03 apfu, CO_2 is 0.99 apfu and F is 0.98 apfu (Table 4).

Vasyukova, O.V., Williams-Jones, A.E., 2016. The evolution of immiscible silicate and fluoride melts: implications for REE ore-genesis. Geochimica et Cosmochimica Acta 172, 205-224. DOI:10.1016/j.gca.2015.09.018

The gagarinite-(Y) (4 analyses) contains 55±2 wt.% total REE, including 13.5±1.2 wt.% Y_2O_3, 31.6±0.5 wt.% F, 17.7±0.2 wt.% Ca, and 7.0±1.9 wt.% Na_2O (Table 3). In contrast to the REE minerals described earlier, the gagarinite-(Y) is depleted in the LREE and enriched in the middle REE, e.g., Sm and Gd (Fig. 8). Its composition deviates slightly from the ideal mineral formula of $(Na(REE_xCa_{1-x})(REE_yCa_{1-y})F_6)$ because of a deficiency in Na. Assuming 6 fluorine atoms per formula unit, it contains 0.81 apfu Na, 1.3 apfu REE and 1.14 apfu Ca (Table 4). The Na deficiency can be explained by the substitution of REE^{3+} and Na^+ by $2Ca^{2+}$.

Analyses of fluorite (8 crystals) show that the cores (4 analyses) contain 2.9±1.3 wt.% REE, and 0.7±0.6 wt.% Na_2O and the rims (4 analyses) 8±1.3 wt.% REE, and 1.9±0.3 wt.% Na_2O (Table 2). The chondrite-normalised REE profiles are flat and parallel; fluorite rims are enriched in all REE (Fig 8). Both profiles display minor enrichment in Nd (Fig. 8). Fluorite formulae based on these analyses are presented in Table 4.

The cores of zircon crystals (16 analyses) contain 5.6±1.0 wt.% HREE, including 4.8±1.0 wt.% Y_2O_3, whereas their rims (40 analyses) only contain 1.5±0.8 wt.% HREE, including 1.2±0.6 wt.% Y_2O_3 (Table 2). Consequently, the chondrite-normalised REE profiles differ significantly between core and rim (Fig. 8); the REE profiles of the cores are flat, whereas those for the rims have a positive slope and are very similar to those of zircon from the host granite (Fig. 8). Formulae for zircon cores and rims are presented in Table 4.

Discussion

Origin of the inclusion

The extraordinarily high contents of REE, Ca and F (25.08 wt.%, 6.5wt.% and 6.4 wt.%, respectively) and unusual mineralogy of the inclusion indicate that it could not have crystallised

Vasyukova, O.V., Williams-Jones, A.E., 2016. The evolution of immiscible silicate and fluoride melts: implications for REE ore-genesis. Geochimica et Cosmochimica Acta 172, 205-224. DOI:10.1016/j.gca.2015.09.018

from an early silicate melt, as these melts were characterised by modest contents of REE and extremely low Ca and F contents (Vasyukova and Williams-Jones, 2014). The observation of crystals of perthite and quartz protruding from the host granite into the inclusion (Fig. 4a) shows that it is not a xenolith. Instead, this observation indicates that the inclusion must have been at least partly liquid at the time of crystallisation of the protruding minerals. As the only liquid present during the early crystallisation of the Strange Lake pluton, which had a high content of Ca and F, was an immiscible fluoride melt (Vasyukova and Williams-Jones, 2014), we therefore propose that the inclusion formed from this melt. Moreover, as the inclusion is hosted by hypersolvus granite, we further propose that the fluoride melt developed early in the emplacement history of the Strange Lake pluton.

Magmatic crystallisation

As reported above, the REE mineral assemblage changes systematically from the core to the rim of the inclusion, i.e., from fluorite and fluorbritholite-(Ce) (±bastnäsite-(Ce) R and locally fluocerite-(Ce)) in the core to fluorite and a fine-grained REE-rich intergrowth (bastnäsite-(Ce) I, gagarinite -(Y), fluorite and quartz) in the transition zone and to chevkinite-(Ce)-fluorite in the rim (Fig. 3). By contrast, zircon is evenly distributed across the zones, as are quartz and perthite; arfvedsonite is restricted to the core. The textural relationships between REE mineral assemblages and silicate minerals are consistent and independent of the zonal distribution of REE minerals, i.e., the REE minerals are intermixed with perthite, and occur as inclusions in quartz (and arfvedsonite in the core) or fill embayments in these minerals. However, the grain-size of the silicate minerals increases from the core towards the rim.

We propose that the silicate minerals observed within the inclusion crystallised from the silicate melt, which surrounded the fluoride globule, and did so along the boundary between the

Vasyukova, O.V., Williams-Jones, A.E., 2016. The evolution of immiscible silicate and fluoride melts: implications for REE ore-genesis. Geochimica et Cosmochimica Acta 172, 205-224. DOI:10.1016/j.gca.2015.09.018

two melts, because the latter constituted a zone of high energy and steep chemical potential gradients that favoured nucleation and growth of minerals. As growth of these silicate crystals proceeded, the resulting solids deformed the globule of fluoride melt, producing bays and salients, and ultimately incorporated silicate crystals mechanically within the still liquid globule. In consequence, the boundary moved progressively outwards and the overall volume of the inclusion increased. Owing to prolonged crystallisation, the silicate melt adjacent to the boundary became gradually enriched in incompatible elements including volatiles that decreased its viscosity and increased diffusion rates, thus providing for crystallisation of progressively larger crystals.

Zircon is also interpreted to have crystallised from the silicate melt along the boundary between the two melts and was probably the earliest crystallising phase. This interpretation is consistent with the occurrence of unaltered zircon as inclusions in perthite crystals throughout the inclusion. It is also consistent with an observation of the melt inclusion study (Vasyukova and Williams-Jones, 2014) that Zr fractionated preferentially into the silicate melt.

Only two of the REE minerals are interpreted to be primary or magmatic, namely chevkinite-(Ce) and fluorbritholite-(Ce). Chevkinite-(Ce) is found exclusively in the inclusion, mostly within its rim zone, and is not observed in the host granite. Indeed, it has not been observed anywhere else in the Strange Lake pluton by ourselves or other researchers (Miller, 1986, 1990; Salvi and Williams-Jones, 1990; Birkett et al., 1992; Boily and Williams-Jones, 1994; Miller, 1996; Jambor et al., 1998; Salvi and Williams-Jones, 2006; Gysi and Williams-Jones, 2013). We propose that restriction of chevkinite-(Ce) mainly to the rim zone is due to the fact that its crystallisation depended on a supply of Ti, Fe, Zr and Nb from the silicate melt and REE from the fluoride melt. This was only possible at the boundary of the two melts, and

Vasyukova, O.V., Williams-Jones, A.E., 2016. The evolution of immiscible silicate and fluoride melts: implications for REE ore-genesis. Geochimica et Cosmochimica Acta 172, 205-224. DOI:10.1016/j.gca.2015.09.018

explains why chevkinite-(Ce) is present mainly in the rim zone. The occurrence of chevkinite-(Ce) in the transition zone, where it forms inclusions and fills embayments in the quartz (Fig. 4d), may indicate local migration of the rim zone inwards. Crystallisation of chevkinite-(Ce) likely post-dated crystallisation of zircon and perthite, as it is commonly interstitial to perthite and has been observed surrounding zircon (Fig. 4c). This is also consistent with its high content of Ti, Fe and Nb and indicates that the silicate melt surrounding the inclusion was enriched in incompatible elements, due probably to prolonged crystallisation of perthite, arfvedsonite and quartz. Fluorbritholite-(Ce) crystallised away from the silicate melt boundary, exclusively from the fluoride melt, which is interpreted to have remained liquid until after the silicate phases had largely crystallised.

Hydrothermal alteration

Evidence of hydrothermal alteration is particularly strong for the REE minerals. In the core of the inclusion, fluorbritholite-(Ce) was partially altered to bastnäsite-(Ce) R, particularly adjacent to the transition zone. This alteration is interpreted to have occurred according to the reaction:

$$\underset{Fluorbritholite-(Ce)}{\mathrm{REE_{3.6}Ca_{0.8}Na_{0.4}(SiO_4)_3F_{1.2}}} + 2.4\mathrm{F^-} + 4\mathrm{HCO_3^-} + 8\mathrm{H^+} = \underset{Bastnäsite-(Ce)R}{4(\mathrm{REE_{0.9}Ca_{0.1}})(\mathrm{CO_3})\mathrm{F_{0.9}}} + \underset{Quartz}{3\mathrm{SiO_2}} + 0.4\mathrm{Na^+} + 0.4\mathrm{Ca^{2+}} + 6\mathrm{H_2O} \quad (1)$$

Locally within the transition zone, fluorbritholite-(Ce) was replaced by fluocerite-(Ce) and both minerals in turn by bastnäsite-(Ce) R. The replacement of fluorbritholite-(Ce) by fluocerite-(Ce) is interpreted to have occurred via the reaction:

Vasyukova, O.V., Williams-Jones, A.E., 2016. The evolution of immiscible silicate and fluoride melts: implications for REE ore-genesis. Geochimica et Cosmochimica Acta 172, 205-224. DOI:10.1016/j.gca.2015.09.018

$$\underset{Fluorbritholite-(Ce)}{\mathrm{REE_{3.6}Ca_{0.8}Na_{0.4}(SiO_4)_3F_{1.2}}} + 9.6\mathrm{F^-} + 12\ \mathrm{H^+}$$

$$= \underset{Fluocerite-(Ce)}{3.6\mathrm{REEF_3}} + \underset{Quartz}{3\mathrm{SiO_2}} + 0.4\mathrm{Na^+} + 0.8\mathrm{Ca^{2+}} + 6\mathrm{H_2O} \qquad (2)$$

399 The dominant alteration within the transition zone was the replacement of bastnäsite-(Ce) R
400 by an intergrowth of bastnäsite-(Ce) I, gagarinite-(Y) and fluorite according to the reaction:

$$\underset{Bastn\ddot{a}site-(Ce)R}{\mathrm{(REE_{0.9}Ca_{0.1})(CO_3)F_{0.9}}} + 1.8\ \mathrm{F^-} + 0.2\mathrm{Na^+} + 0.5\mathrm{H^+}$$

$$= \underset{Gagarinite-(Y)}{0.3\mathrm{Na_{0.8}REE_{1.3}Ca_{1.1}F_6}} + \underset{Bastn\ddot{a}site-(Ce)I}{0.5\mathrm{REE(CO_3)F}} + \underset{Fluorite}{0.2\ \mathrm{CaF_2}} + 0.5\mathrm{HCO_3^-} \qquad (3)$$

401 Alteration of chevkinite-(Ce) crystals in the rim zone was minimal. Where observed, it is
402 evident as irregular patches of karnasurtite-(Ce) or a fine-grained intergrowth of bastnäsite-(Ce),
403 gagarinite-(Y) and fluorite.

404 In addition to the REE minerals, zircon also shows evidence of extensive hydrothermal
405 alteration in all zones of the inclusion as well as in the host granite. The alteration of zircon
406 occurred in two steps (Fig. 7). In the first step, anhydrous Na-, K-, or Ca-zirconosilicates
407 replaced zircon according to the reactions:

$$\underset{Zircon}{ZrSiO_4} + 2Na^+ + \underset{Quartz}{3SiO_2} + H_2O = \underset{Vlasovite}{Na_2ZrSi_4O_{11}} + 2H^+ \qquad (4-1)$$

408

$$\underset{Zircon}{ZrSiO_4} + 2K^+ + \underset{Quartz}{5SiO_2} + H_2O = \underset{Dalyite}{K_2ZrSi_6O_{15}} + 2H^+ \qquad (4-2)$$

409

$$\underset{Zircon}{ZrSiO_4} + Na^+ + 0.5Ca^{2+} + \underset{Quartz}{2SiO_2} + 3H_2O$$

$$= \underset{Catapleiite}{NaCa_{0.5}ZrSi_3O_9 \bullet 2(H_2O)} + 2H^+ \qquad (4-3)$$

410 This was followed by replacement of the anhydrous zirconosilicates by elpidite according
411 to the reactions:

Vasyukova, O.V., Williams-Jones, A.E., 2016. The evolution of immiscible silicate and fluoride melts: implications for REE ore-genesis. Geochimica et Cosmochimica Acta 172, 205-224. DOI:10.1016/j.gca.2015.09.018

$$\underset{\text{Vlasovite}}{Na_2ZrSi_4O_{11}} + 3H_2O + \underset{\text{Quartz}}{2SiO_2} = \underset{\text{Elpidite}}{Na_2ZrSi_6O_{15} \cdot 3(H_2O)} \quad (5-1)$$

$$\underset{\text{Dalyite}}{K_2ZrSi_6O_{15}} + 2Na^+ + 3H_2O = \underset{\text{Elpidite}}{Na_2ZrSi_6O_{15} \cdot 3(H_2O)} + 2K^+ \quad (5-2)$$

$$\underset{Catapleiite}{NaCa_{0.5}ZrSi_3O_9 \bullet 2(H_2O)} + Na^+ + H_2O + \underset{\text{Quartz}}{3SiO_2} = \underset{\text{Elpidite}}{Na_2ZrSi_6O_{15} \cdot 3(H_2O)} + 0.5Ca^{2+} \quad (5-3)$$

Similar alteration was reported by Birkett et al. (1992) for the hypersolvus granite, suggesting that the source of the altering fluid was not the inclusion (the fluoride melt) but rather the host granite (the silicate melt). As chevkinite-(Ce) (a rim zone mineral) is relatively unaltered, we conclude that it was more resistant to alteration than the other minerals discussed above.

Arfvedsonite does not show any sign of having been altered, probably because it is only found in the core where alteration was minor. Perthite crystals were albitised along their rims in all zones as well as in the host granite. The relatively modest alteration of the perthite is in strong contrast to the locally pervasive alteration of REE minerals and zircon, and may reflect the much larger grain-size of the perthite, which permitted the development of thick albite rims, thereby protecting the cores from further alteration.

Modal mineralogy and composition of the initial fluoride melt

From the bulk composition of the inclusion, it is possible to roughly estimate the initial (unaltered) modal mineralogy of the inclusion and initial composition of the fluoride melt. This is because many of the major elements can be largely accounted for by a single mineral. Thus, most of the K is accounted for by perthite, the Fe by arfvedsonite, the Zr by zircon, and the Ti by chevkinite-(Ce). It should be noted, however, that the reliability of the estimate depends heavily on the extent to which there was exchange of elements between the inclusion and the host granite. We have assumed that such exchange was minimal, an assumption that is supported in

Vasyukova, O.V., Williams-Jones, A.E., 2016. The evolution of immiscible silicate and fluoride melts: implications for REE ore-genesis. Geochimica et Cosmochimica Acta 172, 205-224. DOI:10.1016/j.gca.2015.09.018

431 the case of the REE by the fact that there is no evidence of enrichment of the REE in the
432 surrounding granite (e.g., the presence of secondary REE minerals), despite the very high
433 concentration of the REE in the inclusion and the fact that the REE minerals show the most
434 evidence of hydrothermal alteration. This assumption is also supported by the observation that
435 the two principal silicate minerals perthite and arfvedsonite show little or no evidence of
436 alteration, respectively (only the rims of perthite crystals have been albitised and the arfvedsonite
437 shows no evidence of replacement by aegirine, the main phase to which it alters elsewhere in the
438 pluton).

439 The relative proportions of the above minerals in the inclusion were calculated by dividing
440 the concentration of their identifying elements in the bulk inclusion by the concentration of these
441 elements in the corresponding minerals. These proportions, in turn, were used to assess the
442 contributions of these minerals to other elements in the bulk inclusion. Thus, by dividing the
443 K_2O content of the bulk inclusion by the average K_2O content in perthite (calculated as 60 wt.%
444 microcline and 40 wt.% albite), we estimated that the inclusion contains 19.4 wt.% perthite
445 (APPENDICES B and C, step 1). The proportions of zircon, chevkinite-(Ce) and arfvedsonite
446 were similarly estimated to be 1.6, 3.8 and 5.2 wt.%, respectively (APPENDIX C, steps 1 and 2).
447 The proportions of Al_2O_3 and Ce_2O_3 remaining after accounting for them in perthite and
448 chevkinite-(Ce), respectively, were assigned to albite and fluorbritholite-(Ce), yielding
449 proportions of these minerals of 3.7 and 38.3 wt.%, respectively (APPENDIX C, step 3).
450 Similarly, the proportion of CaO remaining after accounting for its presence in chevkinite-(Ce)
451 and fluorbritholite-(Ce) was assigned to fluorite. The proportion of fluorite so calculated was 7.0
452 wt.% (APPENDIX C, step 4). The proportion of quartz was determined from that of SiO_2
453 remaining after accounting for the proportions of this oxide in perthite, albite, arfvedsonite,

Vasyukova, O.V., Williams-Jones, A.E., 2016. The evolution of immiscible silicate and fluoride melts: implications for REE ore-genesis. Geochimica et Cosmochimica Acta 172, 205-224. DOI:10.1016/j.gca.2015.09.018

454 fluorbritholite-(Ce), chevkinite-(Ce) and zircon, and is 14.4 wt.% (APPENDIX C, step 5). After
455 these assignments, the proportions of elements in the inclusion that were not accounted for were
456 close to zero (±0.2 wt.%) except for F, which was +2.1 wt.% (APPENDIX C, RC in step 5). This
457 implies that, except in respect to F, the calculated mineral proportions accurately reflect the
458 initial modal mineralogy of the inclusion. The fact that the amount of F in the inclusion exceeds
459 the amount of F that can be accounted for by the minerals considered in our calculations suggests
460 that the F content changed during alteration. This is consistent with our earlier assumption that F
461 was partly added during alteration (see reactions 1-3).

462 In order to calculate the composition of the fluoride melt, contents of elements that
463 comprised the silicate minerals, i.e., perthite, albite, zircon, arfvedsonite and quartz (APPENDIX
464 B) were subtracted from the bulk composition of the inclusion, assuming that the silicate
465 minerals crystallized from the silicate melt (APPENDIX D). In the case of chevkinite-(Ce), it
466 was assumed that Ti, Fe, Zr, Nb and Si were furnished by the silicate melt and the REE by the
467 fluoride melt (APPENDIX D). Converted to element wt.% and normalized to 100 %, the
468 composition of the fluoride melt so-calculated is 9.4 wt.% Si, 11.2 wt.% Ca, 1.2 wt.% Na, 15.4
469 wt.% F, 2.9 wt.% Y, 13.4 wt.% La, 26.4 wt.% Ce, 3.0 wt.% Pr, 10.5 wt.% Nd, 2.0 wt.% Sm, 1.5
470 wt.% Gd and 1.3 wt.% other heavy REE (Table 5).

471 The calculated REE content of the fluoride melt composition is very similar to that of the
472 REE-rich fluoride melt trapped in type 3 melt inclusions (Vasyukova and Williams-Jones, 2014),
473 i.e., 2.9 wt.% Y, 13.4 wt.% La, 26.4 wt.% Ce and 10.5 wt.% Nd in the inclusion versus 2.5 wt.%
474 Y, 12.3 wt.% La, 23.0 wt.% Ce and 7.9 wt.% Nd in the type 3 melt (Table 5). However, the
475 contents calculated for other elements in the fluoride melt differ significantly from those
476 measured in the type 3 melt inclusions. The differences are greatest for F and Si. Whereas, the

Vasyukova, O.V., Williams-Jones, A.E., 2016. The evolution of immiscible silicate and fluoride melts: implications for REE ore-genesis. Geochimica et Cosmochimica Acta 172, 205-224. DOI:10.1016/j.gca.2015.09.018

type 3 melt inclusions contain 38.8 wt.% F and 0.2 wt.% Si on average, the fluoride melt forming the inclusion is estimated to have contained 15.4 wt.% F and 9.4 wt.% SiO_2 (Table 5). The fact that unheated type 3 inclusions contained fluorite and gagarinite, whereas the inclusion discussed in this paper crystallised to fluorbritholite-(Ce), indicates that type 3 inclusions were Si-poor and F-rich, and the fluoride melt in the inclusion was Si-rich and relatively poor in F. This means that the differences in composition cannot be an artifact of the heating and quenching of the type 3 inclusions in the laboratory. Neither can they be explained by diffusion of Si and F from or into the melt inclusions, respectively, after entrapment, but prior to being heated. This is because both elements would have diffused down their chemical potential gradients, i.e., Si would have diffused from the quartz host into the inclusions and F from the inclusions into the quartz host. Consequently the melt inclusions would have been enriched in Si and depleted in F, which is opposite to what would be needed to explain the compositional differences discussed above. The only reasonable explanation for the difference between the Si and F contents measured in the type 3 inclusions and those calculated for the fluoride melt in the inclusion studied in this paper is that they reflect different stages in the evolution of the fluoride melt. As the fluoride melt investigated in this study was present prior to crystallisation of perthite, an early phase in the hypersolvus granite, and the fluoride melt in the type 3 melt inclusions was trapped in quartz, a late crystallising mineral, it is possible and, indeed, probable that they represent less and more evolved aliquots of the fluoride melt, respectively. Significantly, fluorine forms sodium fluoride complexes in Al-poor silicate melts (Mysen and Virgo, 1985a, b), which enables silicate magmas of the type present at Strange Lake (peralkaline) to dissolve high concentrations of fluorine. When arfvedsonite joined the liquidus at a relatively late stage of crystallisation (arfvedsonite occurs interstitially to perthite), it consumed Na from the melt and that destabilised the sodium

Vasyukova, O.V., Williams-Jones, A.E., 2016. The evolution of immiscible silicate and fluoride melts: implications for REE ore-genesis. Geochimica et Cosmochimica Acta 172, 205-224. DOI:10.1016/j.gca.2015.09.018

fluoride complexes, thereby liberating F to the exsolving fluoride melt and displacing Si from it. Thus, the type 3 inclusions could have trapped late exsolving fluoride melt, enriched in fluorine and depleted in silica, which was not present during formation of the inclusion studied in this paper.

Genetic model

Based on the observations that have been presented above, we can confidently conclude that the inclusion described in this paper formed from a globule of fluoride melt that exsolved from a peralkaline granitic magma. As this globule was discovered in the earliest and least evolved of the granites, we can also conclude that this immiscibility occurred early in the emplacement history of the Strange Lake pluton. Finally, we can conclude that Ca, F and the REE partitioned into the fluoride melt, whereas Ti, Zr, and Nb remained in the silicate melt.

During crystallisation, the boundary between the two melts acted as a locus of nucleation and crystal growth because of the high energy of the boundary relative to that of the adjacent melts, and the steep chemical potential gradients. As a result, crystals formed earlier along this boundary than within either the silicate or fluoride melt. The first crystals to form were zircon followed by perthite, both crystallised from the silicate melt (Fig. 10a). During growth, these crystals deformed the fluoride melt, creating bays and salients along its border, and ultimately became mechanically incorporated within the body of the fluoride melt (Fig. 10b). The melt boundary moved progressively outwards and the volume of the globule increased (see red dashed line representing the initial boundary in Fig. 10). Owing to prolonged crystallisation, the silicate melt around the globule became gradually more enriched in volatiles, which lead to a decrease in melt viscosity and facilitated crystallisation of progressively larger crystals, i.e., large

Vasyukova, O.V., Williams-Jones, A.E., 2016. The evolution of immiscible silicate and fluoride melts: implications for REE ore-genesis. Geochimica et Cosmochimica Acta 172, 205-224. DOI:10.1016/j.gca.2015.09.018

arfvedsonite and feldspar crystals around the aplitic zone (Fig. 10c) and even larger amoeboid-shaped quartz crystals in the transition zone (Fig. 10d). Crystallisation of chevkinite-(Ce) started before that of the large amoeboid-shaped quartz crystals, and did so from both the silicate and fluoride melt, with the former furnishing Ti, Fe, Zr and Nb and the fluoride melt the REE. Wholesale crystallisation of the fluoride melt, however, occurred late, largely post-dating crystallisation of the silicate minerals of the inclusion, and involved crystallisation of fluorbritholite-(Ce) and fluorite in interstices between perthite, arfvedsonite and quartz.

Exsolution of a hydrothermal fluid occurred during crystallisation of the hypersolvus granite. This fluid invaded the inclusion and altered minerals within it. Fluorbritholite-(Ce) was replaced by fluocerite-(Ce) and then by bastnäsite-(Ce) R, which, in turn, was replaced by a fine-grained intergrowth of bastnäsite-(Ce) I, gagarinite-(Y) and fluorite, and zircon was altered to anhydrous Na-K-Ca zirconosilicates and subsequently to elpidite.

The role of silicate-fluoride immiscibility in REE mineralisation

In our previous publication, we estimated the proportion of fluoride melt that could account for the REE content of the Strange Lake granites and pegmatites (Table 5 inVasyukova and Williams-Jones, 2014). The calculation assumed that most of the fluoride melt had the composition of type 2 melt inclusions (Ca-fluoride) and showed that the REE budget of the hypersolvus granite, the subsolvus granite and the pegmatites could be accounted for by 2.7 wt.%, 6.0 wt.% and 12.1 wt.% fluoride melt, respectively. If, on the other hand, the fluoride melt had the REE content of the type 3 melt inclusions (which is the case for the inclusion discussed in this paper), then only 0.5, 1.1 and 2.3 wt.% of fluoride melt would be required to explain the bulk REE contents of the above intrusive phases, respectively (Table 6). However, in this

Vasyukova, O.V., Williams-Jones, A.E., 2016. The evolution of immiscible silicate and fluoride melts: implications for REE ore-genesis. Geochimica et Cosmochimica Acta 172, 205-224. DOI:10.1016/j.gca.2015.09.018

544 calculation, the HREE content is underestimated because the type 3 melt (and the inclusion; Fig.
545 8) is depleted in Y (and therefore other HREE) compared to the type 2 melt (Table 5 in
546 Vasyukova and Williams-Jones, 2014). Given that the fluoride melt was a mix of the Ca-fluoride
547 (type 2) and REE-fluoride (type 3) melts, and to account for the low HREE content of the REE-
548 fluoride melt, we consider that values intermediate between those reported in Vasyukova and
549 Williams-Jones (2014) and those calculated above, provide the most realistic estimates of the
550 proportions of fluoride melt responsible for the REE contents of the different granite types.

551 ## Conclusions

552 Melt inclusions from the Strange Lake granites previously studied by us (Vasyukova and
553 Williams-Jones, 2014) provided evidence for silicate-fluoride immiscibility and showed that this
554 process played a major role in concentrating REE in the pegmatites. However, these inclusions
555 represent melts trapped during a brief interval late in the crystallisation history of the
556 hypersolvus granite, and thus they only furnished limited information on this history, particularly
557 regarding the REE mineralisation. By contrast, the inclusion described in this paper preserved
558 evidence of the primary crystallisation sequence at the interface between silicate and fluoride
559 melts that allowed us to reconstruct the history of these melts from the earliest stages of their
560 separation to the latest stages of hydrothermal alteration. We now know that as soon as the
561 fluoride melt exsolved, it began scavenging REE from the silicate melt, and that the boundary
562 between the melts acted as a locus of nucleation facilitating early crystallisation of minerals. This
563 unusual environment afforded a unique set of crystallisation conditions that allowed formation of
564 chevkinite-(Ce), which took up elements from both silicate and fluoride melts. As a result of
565 their cooling and crystallisation, immiscible fluoride globules locked up the REE, F and Ca

Vasyukova, O.V., Williams-Jones, A.E., 2016. The evolution of immiscible silicate and fluoride melts: implications for REE ore-genesis. Geochimica et Cosmochimica Acta 172, 205-224. DOI:10.1016/j.gca.2015.09.018

preventing their dispersion within the silicate melt until the late hydrothermal stage when they were again redistributed. Although the deposit as we observe it now only preserves the record of this hydrothermal remobilisation, the results of this study provide compelling evidence that silicate-fluoride immiscibility was the dominant process concentrating the REE to potentially economic levels.

Acknowledgements

The research presented in this paper was funded by a NSERC Discovery and Industry Collaborative grant (Quest Rare Minerals Ltd.) and a FQRNT team grant. Quest Rare Minerals president, P. Cashin, and exploration team members, P. Guay and P. Collins supplied valuable input and access to essential data. We are particularly grateful to P. Collins and A. Buchanan who discovered and generously donated the inclusion on which this study was based. L. Shi provided important advice on the EMP analysis of REE minerals and zircon. We thank Adam Simon and the anonymous reviewer for their insightful comments and suggestions.

Vasyukova, O.V., Williams-Jones, A.E., 2016. The evolution of immiscible silicate and fluoride melts: implications for REE ore-genesis. Geochimica et Cosmochimica Acta 172, 205-224. DOI:10.1016/j.gca.2015.09.018

References

Birkett, T.C., Miller, R.R., Roberts, A.C., Mariano, A.N., 1992. Zirconium-bearing minerals of the Strange Lake intrusive complex, Quebec Labrador. Can Mineral 30, 191-205.

Boily, M., Williams-Jones, A.E., 1994. The role of magmatic and hydrothermal processes in the chemical evolution of the Strange Lake plutonic complex, Quebec-Labrador. Contrib Mineral Petr 118, 33-47.

Gysi, A.P., Williams-Jones, A.E., 2013. Hydrothermal mobilization of pegmatite-hosted REE and Zr at Strange Lake, Canada: A reaction path model. Geochimica et Cosmochimica Acta 122, 324-352.

Jambor, J.L., Roberts, A.C., Grice, J.D., Birkett, T.C., Groat, L.A., Zajac, S., 1998. Gerenite-(Y),$(Ca,Na)_2(Y,REE)_3Si_6O_{18}\bullet 2H_2O$, a new mineral species, and an associated Y-bearing gadolinite-group mineral, from the Strange Lake peralkaline complex, Quebec-Labrador. Can Mineral 36, 793-800.

Klemme, S., 2004. Evidence for fluoride melts in earth's mantle formed by liquid immiscibility. Geology 32, 441-444.

Mcdonough, W.F., Sun, S.S., 1995. The Composition of the Earth. Chemical Geology 120, 223-253.

Vasyukova, O.V., Williams-Jones, A.E., 2016. The evolution of immiscible silicate and fluoride melts: implications for REE ore-genesis. Geochimica et Cosmochimica Acta 172, 205-224. DOI:10.1016/j.gca.2015.09.018

596 Miller, R.R., 1986. Geology of the Strange Lake Alkalic Complex and the associated Zr-Y-Nb-
597 Be-REE mineralization. Curr. Res. Newfoundland Department Mines Energy Rep. 86, 11-19.

598 Miller, R.R., 1990. The Strange Lake pegmatite-aplite hosted rare-metal deposit, Labrador. Curr.
599 Res. Newfoundland Department Mines Energy Rep. 90, 171-182.

600 Miller, R.R., 1996. Structural and textural evolution of the Strange Lake peralkaline rare-element
601 (NYF) granitic pegmatite, Quebec-Labrador. Can Mineral 34, 349-371.

602 Miller, R.R., Heaman, L.M., Birkett, T.C., 1997. U-Pb zircon age of the Strange Lake
603 peralkaline complex: Implications for Mesoproterozoic peralkaline magmatism in north-central
604 Labrador. Precambrian Res 81, 67-82.

605 Mysen, B.O., Virgo, D., 1985a. Structure and properties of fluorine-bearing aluminosilicate
606 melts - the system Na_2O-Al_2O_3-SiO_2-F at 1 Atm. Contrib Mineral Petr 91, 205-220.

607 Mysen, B.O., Virgo, D., 1985b. Interaction between fluorine and silica in quenched melts on the
608 joins SiO_2-AlF_3 and SiO_2-NaF determined by Raman spectroscopy. Physics and Chemistry of
609 Minerals 12, 77-85.

610 Peretyazhko, I.S., Zagorsky, V.Y., Tsareva, E.A., Sapozhnikov, A.N., 2007. Immiscibility of
611 calcium fluoride and aluminosilicate melts in ongonite from the Ary-Bulak intrusion, Eastern
612 Transbaikal region. Dokl Earth Sci 413, 315-320.

Vasyukova, O.V., Williams-Jones, A.E., 2016. The evolution of immiscible silicate and fluoride melts: implications for REE ore-genesis. Geochimica et Cosmochimica Acta 172, 205-224. DOI:10.1016/j.gca.2015.09.018

613 Salvi, S., Williams-Jones, A.E., 1990. The role of hydrothermal processes in the granite-hosted
614 Zr, Y, Ree deposit at Strange Lake, Quebec Labrador - evidence from fluid inclusions.
615 Geochimica Et Cosmochimica Acta 54, 2403-2418.

616 Salvi, S., Williams-Jones, A.E., 2006. Alteration, HFSE mineralisation and hydrocarbon
617 formation in peralkaline igneous systems: Insights from the Strange Lake Pluton, Canada. Lithos
618 91, 19-34.

619 Vasyukova, O.V., Williams-Jones, A.E., 2014. Fluoride–silicate melt immiscibility and its role
620 in REE ore formation: Evidence from the Strange Lake rare metal deposit, Quebec-Labrador,
621 Canada. Geochimica et Cosmochimica Acta 139, 110-130.

622 Veksler, I.V., Dorfman, A.M., Kamenetsky, M., Dulski, P., Dingwell, D.B., 2005. Partitioning of
623 lanthanides and Y between immiscible silicate and fluoride melts, fluorite and cryolite and the
624 origin of the lanthanide tetrad effect in igneous rocks. Geochimica Et Cosmochimica Acta 69,
625 2847-2860.

626 Veksler, I.V., Dorfman, A.M., Dulski, P., Kamenetsky, V.S., Danyushevsky, L.V., Jeffries, T.,
627 Dingwell, D.B., 2012. Partitioning of elements between silicate melt and immiscible fluoride,
628 chloride, carbonate, phosphate and sulfate melts, with implications to the origin of
629 natrocarbonatite. Geochimica Et Cosmochimica Acta 79, 20-40.

630

Vasyukova, O.V., Williams-Jones, A.E., 2016. The evolution of immiscible silicate and fluoride melts: implications for REE ore-genesis. Geochimica et Cosmochimica Acta 172, 205-224. DOI:10.1016/j.gca.2015.09.018

Captions

Figure 1 A geological map of the Strange Lake pluton, showing the distribution of the principal rock types and the location of the sample on which this study was based.

Figure 2 The mineralogy of the host hypersolvus granite illustrated by backscattered electron (BSE) images; (a), (b) - images showing relationships among the main rock-forming minerals and HFSE/REE minerals, (c) and (d) – enlargements of the areas shown by the rectangles in (b). Image (c) shows relationships among zircon and other zirconosilicate minerals; (d) is an image of an intergrowth of bastnäsite-(Ce), fluorite, albite and quartz. Y - Y-rich inclusions in quartz. Ca-Na-Zr – remnants of vlasovite and catapleiite, K-Na-Zr – remnants of vlasovite and dalyite. Other mineral abbreviations are listed in APPENDIX E.

Figure 3 The REE-rich inclusion that was the focus of this study. (a) - a photograph showing the inclusion in the host hypersolvus granite, (b) - a sketch identifying macroscopic zoning in the inclusion, (c) - a sketch showing the distribution of silicate minerals and REE mineral assemblages in the inclusion.

Figure 4 Textural relationships among minerals in the rim zone illustrated by BSE images; (a) - an image showing the host granite, the rim zone and the transition zone. An embayment in the inclusion filled by the host granite is indicated by the black arrow; (b) - textural relationships among arfvedsonite, aenigmatite and chevkinite-(Ce); (c) - textural relationships among chevkinite-(Ce), zircon, fluorite and a REE-rich intergrowth involving bastnäsite-(Ce), gagarinite-(Y) and fluorite. Note that in some cases, chevkinite-(Ce) grew around zircon (the contact is indicated by the black arrow); (d) - inclusions of chevkinite-(Ce), zircon and fluorite in quartz. REE refers to the fine-grained intergrowth of bastnäsite-(Ce) I, gagarinite-(Y) and fluorite in (c). Other mineral abbreviations are listed in APPENDIX E.

Vasyukova, O.V., Williams-Jones, A.E., 2016. The evolution of immiscible silicate and fluoride melts: implications for REE ore-genesis. Geochimica et Cosmochimica Acta 172, 205-224. DOI:10.1016/j.gca.2015.09.018

Figure 5 Textural relationships among minerals in the transition zone illustrated by BSE images; (a) – an overview showing contacts between the host granite, the rim, the transition zone and the core; (b) – an intergrowth of bastnäsite-(Ce), gagarinite-(Y), fluorite and quartz; (c) – remnants of fluorbritholite-(Ce), fluocerite-(Ce) and bastnäsite-(Ce) R in a matrix of REE-rich intergrowth, (d) – replacement of fluorbritholite-(Ce) by fluocerite-(Ce) and both fluorbritholite-(Ce) and fluocerite-(Ce) by bastnäsite-(Ce) R, (e) – formation of a REE-rich intergrowth at the expense of bastnäsite-(Ce) R. Note the embayment of bastnäsite-(Ce) R by fluorite and incorporation of fluorite in bastnäsite-(Ce) R (shown by the dashed arrow). REE refers to a fine-grained intergrowth of bastnäsite-(Ce) I, gagarinite-(Y) and fluorite, Bst-R refers to bastnäsite-(Ce) R, and Bst-I to bastnäsite-(Ce) I. All other mineral abbreviations used in the figure are listed in APPENDIX E.

Figure 6 Textural relationships among minerals in the core illustrated by BSE images; (a) – a typical image of the core; (b) – the distribution of bastnäsite-(Ce) R and fluorbritholite-(Ce); fluorbritholite-(Ce) is unaltered where it is in contact with arfvedsonite and was altered by bastnäsite-(Ce) R along its contacts with feldspar; (c) – unaltered fluorbritholite-(Ce) and arfvedsonite with inclusions of fluorite; (d) - two types of zircon crystals, a small unaltered euhedral crystal embedded in feldspar and a larger partially altered crystal interstitial between feldspar and fluorbritholite-(Ce). The mineral abbreviations are listed in APPENDIX E.

Figure 7 Images showing the progressive alteration of zircon. (a) and (d) - BSE images. (b) and (e) - X-ray maps showing the distribution of Zr in the areas illustrated in images (a) and (d), respectively. (c) and (f) - images showing the distribution of Ca-Na-, Na- and K-zirconosilicate minerals, zircon, fluorite and quartz in the areas illustrated in (a) and (d), respectively.

Vasyukova, O.V., Williams-Jones, A.E., 2016. The evolution of immiscible silicate and fluoride melts: implications for REE ore-genesis. Geochimica et Cosmochimica Acta 172, 205-224. DOI:10.1016/j.gca.2015.09.018

Figure 8 Chondrite-normalised REE profiles (Mcdonough and Sun, 1995) for the inclusion, the main granite phases and the pegmatites, as well as for selected REE-rich minerals and zircon from the inclusion.

Figure 9 (a) – a BSE image illustrating a zoned chevkinite-(Ce) crystal and the locations of electron microprobe analyses. (b) - a profile through the crystal showing the concentrations of selected oxides based on electron microprobe analyses at the locations indicated in (a).

Figure 10 A schematic model for the primary crystallisation of the inclusion. (a) – crystallisation of perthite followed by that of zircon on the boundary between the silicate melt and the inclusion (fluoride melt); (b) – continued crystallisation of feldspar and zircon and onset of crystallisation of quartz and arfvedsonite, (c) – formation of larger crystals of arfvedsonite and perthite as the silicate melt surrounding the inclusion evolves, (d) - formation of large quartz and perthite crystals from the most evolved melt, large-scale crystallisation of chevkinite-(Ce). 1 - fluoride melt, 2 - silicate melt: a - least evolved, b - more evolved, c - most evolved, 3 - aplite (perthite-rich) zone (core), 4 - zone with large arfvedsonite and perthite crystals, 5 - zone with large amoeboid-like quartz and perthite crystals, 6 - chevkinite-rich zone, 7 - zircon, 8 - perthite, 9 - quartz, 10 - arfvedsonite, 11 - initial fluoride-silicate boundary.

Table 1 Bulk rock composition of the inclusion, the host granite and the average Alterra hypersolvus granite

Table 2 Compositions of primary minerals in the inclusion

Table 3 Compositions of secondary minerals in the inclusion

Table 4 Calculated formulae for selected minerals (apfu)

Table 5 The calculated composition of the fluoride melt in the inclusion compared to the compositions of type 2 and 3 inclusions of Vasyukova and Williams-Jones (2014)

Vasyukova, O.V., Williams-Jones, A.E., 2016. The evolution of immiscible silicate and fluoride melts: implications for REE ore-genesis. Geochimica et Cosmochimica Acta 172, 205-224. DOI:10.1016/j.gca.2015.09.018

699 Table 6 Estimate of the proportion of fluoride melt relative to silicate melt in the
700 hypersolvus/subsolvus granites and pegmatites

701 APPENDIX A Electron microprobe standards, counting times and detection limits used in
702 this study

703 APPENDIX B Mineral compositions used in calculations (wt.%)

704 APPENDIX C The estimated primary modal mineralogy of the inclusion

705 APPENDIX D Calculation of the initial fluoride melt composition compared to that of
706 type 3 inclusions (Vasyukova and Williams-Jones, 2014)

Vasyukova, O.V., Williams-Jones, A.E., 2016. The evolution of immiscible silicate and fluoride melts: implications for REE ore-genesis. Geochimica et Cosmochimica Acta 172, 205-224. DOI:10.1016/j.gca.2015.09.018

Table

Table 1 Bulk rock composition of the inclusion, the host granite and the average Alterra hypersolvus granite

Name	Inclusion	Host granite	Average HYP granite (Alterra, 57 samples)
Wt.%			
SiO_2	41.6	70.9	70.0±0.7
Al_2O_3	4.4	11.5	11.2 ±0.8
Fe_2O_3 (total)	2.1	5.1	4.7±0.3
CaO	6.5	0.9	1.1±0.4
Na_2O	2.8	4.9	5.1±0.5
K_2O	1.7	4.7	4.5±1.1
TiO_2	0.62	0.35	0.30±0.08
P_2O_5	0.03	0.02	0.02±0.01
Nb_2O_5	0.11	0.05	0.10±0.10
ZrO_2	1.0	0.7	0.6±0.2
F	6.4	0.5	0.6±0.2
LOI	7.7	1.1	1.0±0.2
Total	74.9	100.8	98.2±1.0
Ppm and wt.% (*)			
Y	1.24*	521	790±590
La	5.50*	371	410±140
Ce	10.8*	757	960±410
Pr	1.22*	82	110±50
Nd	4.32*	281	390±170
Sm	0.80*	58	94±52
Eu	398	3	6±3
Gd	0.61*	54	90±56
Tb	728	13	20±15
Dy	0.29*	84	140±110
Ho	428	20	30±25
Er	913	59	96±81
Tm	86	10	15±12
Yb	366	63	95±68
Lu	40	9	13±8
Total	25.08*	2385	3260±1790

The uncertainty is reported to 2 standard deviations

Vasyukova, O.V., Williams-Jones, A.E., 2016. The evolution of immiscible silicate and fluoride melts: implications for REE ore-genesis. Geochimica et Cosmochimica Acta 172, 205-224. DOI:10.1016/j.gca.2015.09.018

Table 2 Compositions of primary minerals in the inclusion (wt.%)

Mineral	Chevkinite-(Ce)	Fluorbritholite-(Ce)	Fluorite		Zircon	
			Core	Rim	Core	Rim
Number of analyses	76	30	4	4	16	40
SiO_2	19.8±0.2	21.6±0.6	-	-	32.1±0.4	32.6±0.3
FeO_{Total}	12.2±0.4	0.43±0.06	-	-	-	-
CaO	1.2±0.5	5.3±1.6	69±3	63±1	0.3±0.3	-
Na_2O	-	1.5±0.5	0.7±0.6	1.9±0.3	-	-
TiO_2	16.4±0.7	-	-	-	-	-
Nb_2O_5	2±0.4	-	-	-	-	-
ZrO_2	0.3±0.2	-	-	-	59±1	64±1
HfO_2	-	-	-	-	1.2±0.6	0.4±0.1
F	0.41±0.06	2.8±0.1	45.4±0.3	44.6±0.6	-	-
Y_2O_3	-	3.1±0.4	1.6±1.2	3.7±1.2	4.8±1.0	1.2±0.6
La_2O_3	13.9±0.9	14.8±1.1	0.2±0.2	0.8±0.4	na	na
Ce_2O_3	23.5±0.9	30.7±1.0	0.4±0.4	1.5±0.3	na	na
Pr_2O_3	2.3±0.2	3.6±0.3	0.12±0.05	0.20±0.05	na	na
Nd_2O_3	7.0±0.4	12.2±0.8	0.3±0.3	1.2±0.2	na	na
Sm_2O_3	0.7±0.1	2.1±0.3	0.1±0.1	0.2±0.05	na	na
Gd_2O_3	0.4±0.1	2.3±0.3	0.2±0.2	0.5±0.2	na	na
Dy_2O_3	-	0.5±0.1	-	-	0.3±0.2	0.1±0.1
Er_2O_3	-	-	-	-	0.2±0.1	0.1±0.1
Yb_2O_3	-	-	-	-	0.2±0.2	0.1±0.1
TREO	47.8±1.3	69.2±1.8	2.9±1.3	8.0±1.3	5.6±1.0	1.5±0.6
F=O	0.2	1.2	19.1	18.7	-	-
Total	99.9	99.7	98.9	98.9	98.1	98.5

na – not analysed
The uncertainty is reported to 2 standard deviations

Table 3 Compositions of secondary minerals in the inclusion (wt.%)

Mineral	Bastnäsite-(Ce) R	Fluocerite-(Ce)	Bastnäsite-(Ce) I	Gagarinite-(Y)
Number of analyses	14	5	26	4
SiO_2	1.7±0.6	2.9±1.7	-	-
CaO	3.7±0.5	1.0±0.3	0.5±0.3	17.7±0.2
Na_2O	-	-	-	7.0±1.9
F	7.7±0.8	20±2.1	8.4±0.4	31.6±0.5
BaO	-	0.5±0.2	-	-
SrO	0.37±0.05	0.7±0.4	-	-
Y_2O_3	4.4±0.3	3.2±0.3	0.2±0.2	13.5±1.2
La_2O_3	15.0±0.8	17.3±0.7	18.7±0.8	1.3±0.3
Ce_2O_3	28.2±0.7	37.0±1.2	37.4±0.8	6.7±1.3
Pr_2O_3	3.3±0.3	4.2±0.2	4.2±0.2	1.9±0.3
Nd_2O_3	11.9±0.4	14.1±0.5	12.6±0.5	13.5±0.9
Sm_2O_3	2.0±0.2	2.4±0.2	1.2±0.2	5.9±0.5
Gd_2O_3	2.4±0.2	2.6±0.3	0.6±0.2	9.8±0.8
Dy_2O_3	0.4±0.1	0.43±0.08	-	2.3±0.2
CO_2	21.5±1.9	-	19.5±0.6	-
TREO	67.7±1.2	81.3±1.6	74.9±1.3	55±2
F=O	3.2	8.4	3.5	13.3
Total	99.6	98.1	99.8	97.9

The uncertainty is reported to 2 standard deviations

Vasyukova, O.V., Williams-Jones, A.E., 2016. The evolution of immiscible silicate and fluoride melts: implications for REE ore-genesis. Geochimica et Cosmochimica Acta 172, 205-224. DOI:10.1016/j.gca.2015.09.018

Table 4 Calculated formulae for selected minerals (apfu)

Name	SiO_2	FeO	CaO	Na_2O	TiO_2	Nb_2O_5	ZrO_2	HfO_2	F	LREE (+Y)	HREE (+Y)	CO_2	Total O (F)	Formula
Chevkinite-(Ce)	4.15	2.14	0.26		2.59	0.19	0.03		0.27	3.66			22	$(REE,Ca)_{3.93}(Fe^{2+},Ti,Fe^{3+},Zr,Nb)_{4.95}Si_{4.15}O_{22}$
Fluorbritholite-(Ce)	3.00		0.78	0.39					1.24	3.54			13	$(Ca,REE,Na)_{4.74}(SiO_4)_3F_{1.24}$
Bastnäsite-(Ce) R			0.14						0.83	0.86		1.01	4	$(REE,Ca)(CO_2)_{1.01}F_{0.83}$
Bastnäsite-(Ce) I			0.02						0.98	1.01		0.99	4	$(REE,Ca)_{1.03}(CO_2)_{0.99}F_{0.98}$
Gagarinite-(Y)			1.14	0.81					6.00	1.30			6	$Na_{0.81}REE_{1.3}Ca_{1.14}F_6$
Fluorite-core			1.00	0.02					1.93	0.02			2	$CaNa_{0.02}REE_{0.02}F_{1.93}$
Fluorite-rim			0.93	0.05					1.95	0.05			2	$Ca_{0.93}Na_{0.05}REE_{0.05}F_{1.95}$
Zircon-core	1.02						0.91	0.01			0.09		4	$Zr_{0.91}Hf_{0.01}HREE_{0.09}(SiO_4)_{1.02}$
Zircon-rim	1.01						0.97	0.01			0.02		4	$Zr_{0.97}Hf_{0.01}HREE_{0.02}(SiO_4)_{1.01}$

Vasyukova, O.V., Williams-Jones, A.E., 2016. The evolution of immiscible silicate and fluoride melts: implications for REE ore-genesis. Geochimica et Cosmochimica Acta 172, 205-224. DOI:10.1016/j.gca.2015.09.018

Table 5 The calculated composition of the fluoride melt in the inclusion compared to the compositions of type 2 and 3 inclusions of Vasyukova and Williams-Jones (2014)

Elements	Inclusion fluoride melt, wt.%	Type 3 inclusions, average (5 analyses), wt.%	Type 2 inclusions, average (9 analyses), wt.%
Si	9.4	0.2	0.2
Al	-	bdl	bdl
Fe	0.8	bdl	bdl
Ca	11.2	12.5	41.0
Na	1.2	2.7	0.8
K	-	bdl	bdl
Ti	0.9	bdl	bdl
Nb	-	bdl	bdl
Zr	-	bdl	bdl
F	15.4	38.8	47.7
Y	2.9	2.5	3.9
La	13.4	12.3	1.1
Ce	26.4	23.0	2.6
Pr	3.0	na	na
Nd	10.5	7.9	1.6
Sm	2.0	na	na
Eu	0.1	na	na
Gd	1.5	na	na
Tb	0.2	na	na
Dy	0.7	na	na
Ho	0.1	na	na
Er	0.2	na	na
Tm	0.02	na	na
Yb	0.1	na	na
Lu	0.01	na	na

Vasyukova, O.V., Williams-Jones, A.E., 2016. The evolution of immiscible silicate and fluoride melts: implications for REE ore-genesis. Geochimica et Cosmochimica Acta 172, 205-224. DOI:10.1016/j.gca.2015.09.018

Table 6 Estimate of the proportion of fluoride melt relative to silicate melt in the hypersolvus/subsolvus granites and pegmatites

Units	REE, wt.%	Wt.% of fluoride melt based on type 2 inclusions (previous study)	Wt.% of fluoride melt based on type 3 inclusions (this study)
Hypersolvus granites	0.25	2.7	0.5
Subsolvus granites	0.55	6.0	1.1
Pegmatite	1.12	12.1	2.3
Fluoride melt type 2	9.25		
Fluoride melt type 3	48.67		

Vasyukova, O.V., Williams-Jones, A.E., 2016. The evolution of immiscible silicate and fluoride melts: implications for REE ore-genesis. Geochimica et Cosmochimica Acta 172, 205-224. DOI:10.1016/j.gca.2015.09.018

APPENDIX A Electron microprobe standards, counting times and detection limits used in this study

Element	Standard	Counting time (s)	Detection limits (ppm) Fluorbritholite-(Ce), Fluorocarbonates, Fluorite, Gagarinite-(Y)	Chevkinite-(Ce)	Zircon
Si	Diopside	20	347	409	391
Ti	Rutile	20		651	
Al	Orthoclase	20	319		
Fe	Fe_2O_3	20		1758	
Ca	Diopside	20	368	363	217
Na	Albite	20	350		
K	Orthoclase	20		289	
F	Fluorite	20	927	1194	
Cl	Vanadinite	20	137	285	227
Zr	Zircon	20		900	889
Hf	Zircon	20			610
Nb	$Na_2Nb_2O_6$	20		970	
P	Apatite	20	435		202
Y	MAC-Y	20	955		648
La	MAC-La	20	1276	1218	
Ce	MAC-Ce	20	1156	1217	
Pr	MAC-Pr	20	2372	2556	
Nd	MAC-Nd	20	2203	2124	
Sm	MAC-Sm	20	2738	2383	
Eu	MAC-Eu	100	5089	1920	
Gd	MAC-Gd	20	4063	2663	
Dy	MAC-Dy	20	3540		518
Er	MAC-Er	20			519
Yb	MAC-Yb	20			1088

Vasyukova, O.V., Williams-Jones, A.E., 2016. The evolution of immiscible silicate and fluoride melts: implications for REE ore-genesis. Geochimica et Cosmochimica Acta 172, 205-224. DOI:10.1016/j.gca.2015.09.018

APPENDIX B Mineral compositions used in calculations (wt.%)

	Perthite	Chevkinite-(Ce)	Zircon	Arfvedsonite	Albite	Fluorbritholite-(Ce)	Fluorite
SiO_2	65.0	19.8	32.5	50.7	67.0	21.6	-
Al_2O_3	19.0	-	-	0.6	20.0	-	-
Fe_2O_3 (total)	-	12.2	-	32.0	-	0.4	-
CaO	-	1.2	-	0.7	-	5.3	62.7
Na_2O	6.0	-	-	9.3	12.0	1.5	
K_2O	8.5	-	-	1.7	-	-	-
TiO_2	-	16.4	-	0.6	-	-	-
Nb_2O_5	-	2.0	-	-	-	-	-
ZrO_2	-	0.3	62.4	0.1	-	-	-
F	-	0.4	-	1.6	-	2.8	44.6
Y_2O_3	-	-	2.2	-	-	3.1	3.7
La_2O_3	-	13.9	-	-	-	14.8	0.8
Ce_2O_3	-	23.5	-	-	-	30.7	1.5
Pr_2O_3	-	2.3	-	-	-	3.6	0.2
Nd_2O_3	-	7.0	-	-	-	12.2	1.2
Sm_2O_3	-	0.7	-	-	-	2.1	0.2
Eu_2O_3	-	-	-	-	-	-	-
Gd_2O_3	-	0.4	-	-	-	2.3	0.5
Tb_2O_3	-	-	-	-	-	-	-
Dy_2O_3	-	-	0.2	-	-	0.4	-
Ho_2O_3	-	-	-	-	-	-	-
Er_2O_3	-	-	0.1	-	-	-	-
Tm_2O_3	-	-	-	-	-	-	-
Yb_2O_3	-	-	0.2	-	-	-	-
Lu_2O_3	-	-	-	-	-	-	-

Vasyukova, O.V., Williams-Jones, A.E., 2016. The evolution of immiscible silicate and fluoride melts: implications for REE ore-genesis. Geochimica et Cosmochimica Acta 172, 205-224. DOI:10.1016/j.gca.2015.09.018

APPENDIX C The estimated primary modal mineralogy of the inclusion

Oxides	Bulk inclusion compo-sition, wt.%	Step 1 Mineral (oxide, amount)[1]			RC[2]	Step 2 Mineral (oxide, amount)[1]	RC[2]	Step 3 Mineral (oxide, amount)[1]		RC[2]	Step 4 Mineral (oxide, amount)[1]	RC[2]	Step 5 Mineral (oxide, amount)[1]	RC[2]
		Perthite (K_2O, 19.4)	Chevkinite-(Ce) (TiO_2, 3.8)	Zircon (ZrO_2, 1.6)		Arfved-sonite, (Fe_2O_3, 5.2)		Albite, (Al_2O_3, 3.7)	Fluorbri-tholite-(Ce), (Ce_2O_3, 38.3)		Fluorite, (CaO, 7.0)		Quartz, (SiO_2, 14.4)	
SiO_2	41.6	12.6	0.8	0.5	27.7	2.6	25.1	2.5	8.3	14.4	-	14.4	14.4	0.0
Al_2O_3	4.4	3.7	0.0	0.0	0.7	0.0	0.7	0.7	0.0	0.0	-	0.0	-	0.0
Fe_2O_3 (total)	2.1	-	0.5	0.0	1.6	1.7	0.0	-	0.2	-0.2	-	-0.2	-	-0.2
CaO	6.5	-	0.0	0.0	6.4	0.0	6.4	-	2.0	4.4	4.4	0.0	-	0.0
Na_2O	2.8	1.2	0.0	0.0	1.6	0.5	1.1	0.4	0.6	0.1	-	0.1	-	0.1
K_2O	1.7	1.6	0.0	0.0	0.0	0.1	-0.1	-	0.0	-0.1	-	-0.1	-	-0.1
TiO_2	0.6	-	0.6	0.0	0.0	0.0	0.0	-	0.0	0.0	-	0.0	-	0.0
Nb_2O_5	0.1	-	0.1	0.0	0.0	0.0	0.0	-	0.0	0.0	-	0.0	-	0.0
ZrO_2	1.0	-	0.0	1.0	0.0	0.0	0.0	-	0.0	0.0	-	0.0	-	0.0
F	6.4	-	0.0	0.0	6.4	0.1	6.3	-	1.1	5.2	3.1	2.1	-	2.1
Y_2O_3	1.6	-	0.0	0.0	1.5	-	1.5	-	1.2	0.3	0.3	0.1	-	0.1
La_2O_3	6.4	-	0.5	0.0	5.9	-	5.9	-	5.7	0.2	0.1	0.2	-	0.2
Ce_2O_3	12.6	-	0.9	0.0	11.7	-	11.7	-	11.8	0.0	0.1	-0.1	-	-0.1
Pr_2O_3	1.4	-	0.1	0.0	1.3	-	1.3	-	1.4	0.0	0.0	-0.1	-	-0.1
Nd_2O_3	5.1	-	0.3	0.0	4.8	-	4.8	-	4.7	0.1	0.1	0.0	-	0.0
Sm_2O_3	0.9	-	0.0	0.0	0.9	-	0.9	-	0.8	0.1	0.0	0.1	-	0.1
Eu_2O_3	0.0	-	0.0	0.0	0.0	-	0.0	-	0.0	0.0	0.0	0.0	-	0.0
Gd_2O_3	0.7	-	0.0	0.0	0.7	-	0.7	-	0.9	-0.2	0.0	-0.2	-	-0.2
Tb_2O_3	0.1	-	0.0	0.0	0.1	-	0.1	-	0.0	0.1	-	0.1	-	0.1
Dy_2O_3	0.3	-	0.0	0.0	0.3	-	0.3	-	0.2	0.2	-	0.2	-	0.2
Ho_2O_3	0.0	-	0.0	0.0	0.0	-	0.0	-	-	0.0	-	0.0	-	0.0
Er_2O_3	0.1	-	0.0	0.0	0.1	-	0.1	-	-	0.1	-	0.1	-	0.1
Tm_2O_3	0.0	-	0.0	0.0	0.0	-	0.0	-	-	0.0	-	0.0	-	0.0
Yb_2O_3	0.0	-	0.0	0.0	0.0	-	0.0	-	-	0.0	-	0.0	-	0.0
Lu_2O_3	0.0	-	-	-	0.0	-	0.0	-	-	0.0	-	0.0	-	0.0

[1] - Mineral used for calculations with the composition shown in APPENDIX B (oxide used in calculations, calculated proportion of mineral in wt.%)
[2] - RC - remaining bulk composition after subtraction of minerals
[3] - Amount of fluorite needed for correction. Corrections were made based on the assumption that all remaining F was due to the consumption of additional fluorite
[4] - Remaining concentration of elements after subtraction of all minerals including additional fluorite. A negative amount of element reflects its loss to the fluid

Vasyukova, O.V., Williams-Jones, A.E., 2016. The evolution of immiscible silicate and fluoride melts: implications for REE ore-genesis. Geochimica et Cosmochimica Acta 172, 205-224. DOI:10.1016/j.gca.2015.09.018

APPENDIX D Calculation of the initial fluoride melt composition compared to that of type 3 inclusions (Vasyukova and Williams-Jones, 2014)

Oxides	Inclusion, wt.%	Inclusion – silicate minerals –Ti – Nb, wt.%	Oxide to elements, wt.%	Melt normalised to 100 wt.%	Type 3 inclusions, averaged (5 analyses), wt.%
SiO_2	41.6	8.3	3.9	9.4	0.2
Al_2O_3	4.4	-	-	-	bdl
Fe_2O_3 (total)	2.1	0.5	0.3	0.8	bdl
CaO	6.5	6.5	4.6	11.2	12.5
Na_2O	2.8	0.7	0.5	1.2	2.7
K_2O	1.7	-	-	-	bdl
TiO_2	0.6	0.6	0.4	0.9	bdl
Nb_2O_5	0.1	-	-	-	bdl
ZrO_2	1.0	-	-	-	bdl
F	6.4	6.3	6.3	15.4	38.8
Y_2O_3	1.6	1.5	1.2	2.9	2.5
La_2O_3	6.4	6.4	5.5	13.4	12.3
Ce_2O_3	12.6	12.6	10.8	26.4	23.0
Pr_2O_3	1.4	1.4	1.2	3.0	na
Nd_2O_3	5.1	5.1	4.3	10.5	7.9
Sm_2O_3	0.9	0.9	0.8	2.0	na
Eu_2O_3	0.05	0.05	0.04	0.1	na
Gd_2O_3	0.7	0.7	0.6	1.5	na
Tb_2O_3	0.1	0.1	0.1	0.2	na
Dy_2O_3	0.3	0.3	0.3	0.7	na
Ho_2O_3	0.05	0.05	0.04	0.1	na
Er_2O_3	0.1	0.1	0.1	0.2	na
Tm_2O_3	0.01	0.01	0.01	0.02	na
Yb_2O_3	0.04	0.04	0.03	0.1	na
Lu_2O_3	0.005	0.005	0.004	0.01	na

Vasyukova, O.V., Williams-Jones, A.E., 2016. The evolution of immiscible silicate and fluoride melts: implications for REE ore-genesis. Geochimica et Cosmochimica Acta 172, 205-224. DOI:10.1016/j.gca.2015.09.018

APPENDIX E List of minerals observed in this study, their ideal formulae and abbreviations used in the Figures

Mineral	Ideal formula	Mineral abbreviations used in Figures
Aenigmatite	$Na_2Fe^{2+}{}_5Ti(Si_6O_{18})O_2$	Aen
Albite	$NaAlSi_3O_8$	Alb
Arfvedsonite	$NaNa_2(Fe^{2+}{}_4Fe^{3+})Si_8O_{22}(OH)_2$	Arf
Astrophyllite	$(K,Na)_3(Fe^{2+},Mn)_7Ti_2Si_8O_{24}(O,OH)_7$	Ast
Bastnäsite-(Ce)	$(Ce,La)(CO_3)F$	Bst
Chevkinite-(Ce)	$(La,Ce,Ca)_4(Fe^{2+},Mn)_2(Ti,Fe^{3+})_3Si_4O_{22}$	Cvk
Dalyite	$K_2ZrSi_6O_{15}$	Dal
Elpidite	$Na_2ZrSi_6O_{15}•3(H_2O)$	Elp
Fluocerite-(Ce)	$(La,Ce)F_3$	FCer
Fluorbritholite-(Ce)	$(Ca,Ce,La,Na)_5(SiO_4,PO_4)_3F$	Fbt
Fluorite	CaF_2	Fl
Gagarinite-(Ce)	$Na(REE_xCa_{1-x})(REE_yCa_{1-y})F_6$	Gg
Gittinsite	$CaZrSi_2O_7$	Gt
Karnasurtite	$(Ce,La,Th)(Ti,Nb)(Al,Fe^{3+})(Si,P)_2O_7(OH)_4•3(H_2O)$	Kar
Perthite	$(Na,K)AlSi_3O_8$	Fsp
Quartz	SiO_2	Qtz
Vlasovite	$Na_2ZrSi_4O_{11}$	Vls
Zircon	$ZrSiO_4$	Zc

Vasyukova, O.V., Williams-Jones, A.E., 2016. The evolution of immiscible silicate and fluoride melts: implications for REE ore-genesis. Geochimica et Cosmochimica Acta 172, 205-224. DOI:10.1016/j.gca.2015.09.018

Figure 1

Click here to download high resolution image

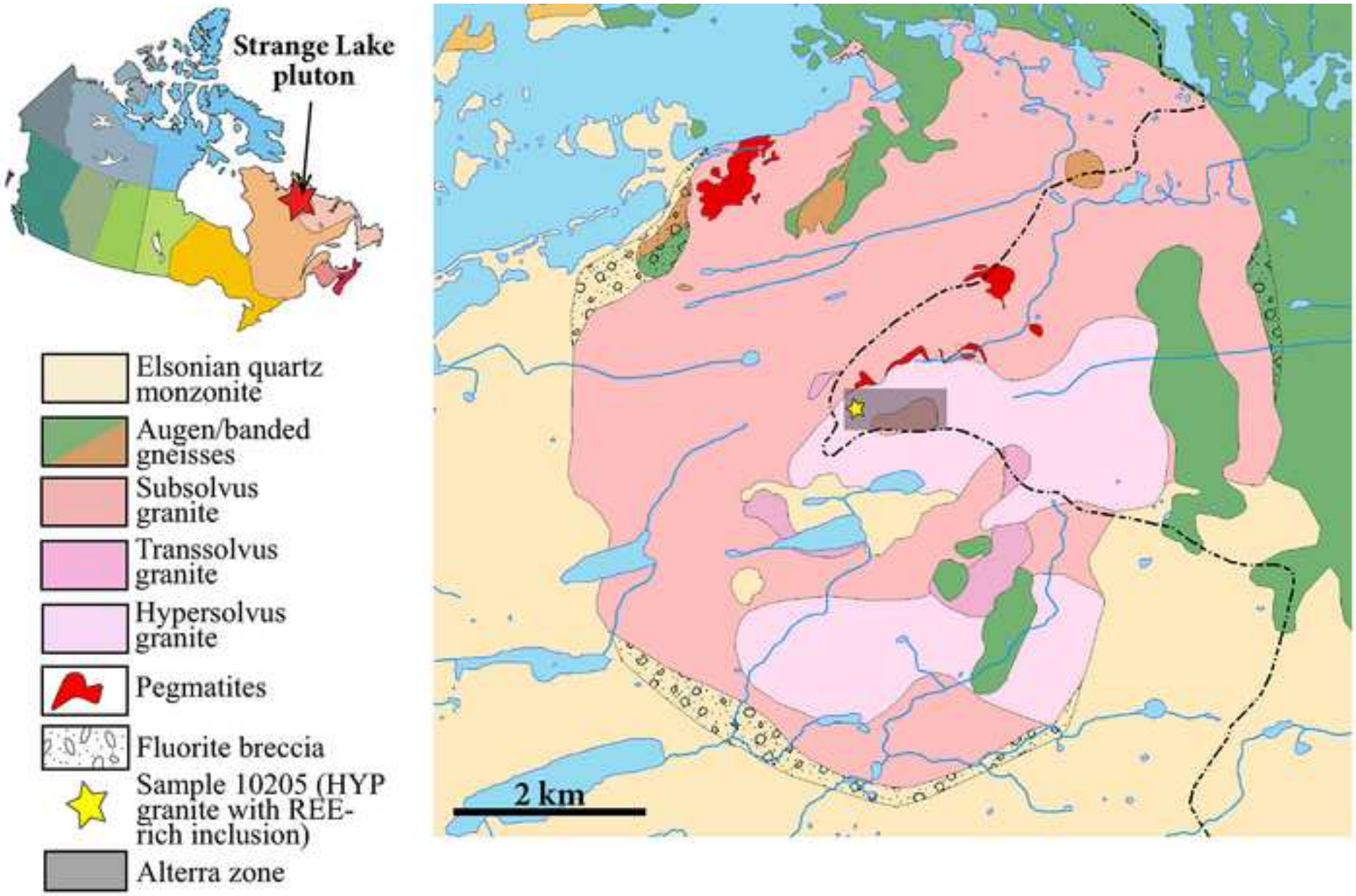

Vasyukova, O.V., Williams-Jones, A.E., 2016. The evolution of immiscible silicate and fluoride melts: implications for REE ore-genesis. Geochimica et Cosmochimica Acta 172, 205-224. DOI:10.1016/j.gca.2015.09.018

Figure 2

Click here to download high resolution image

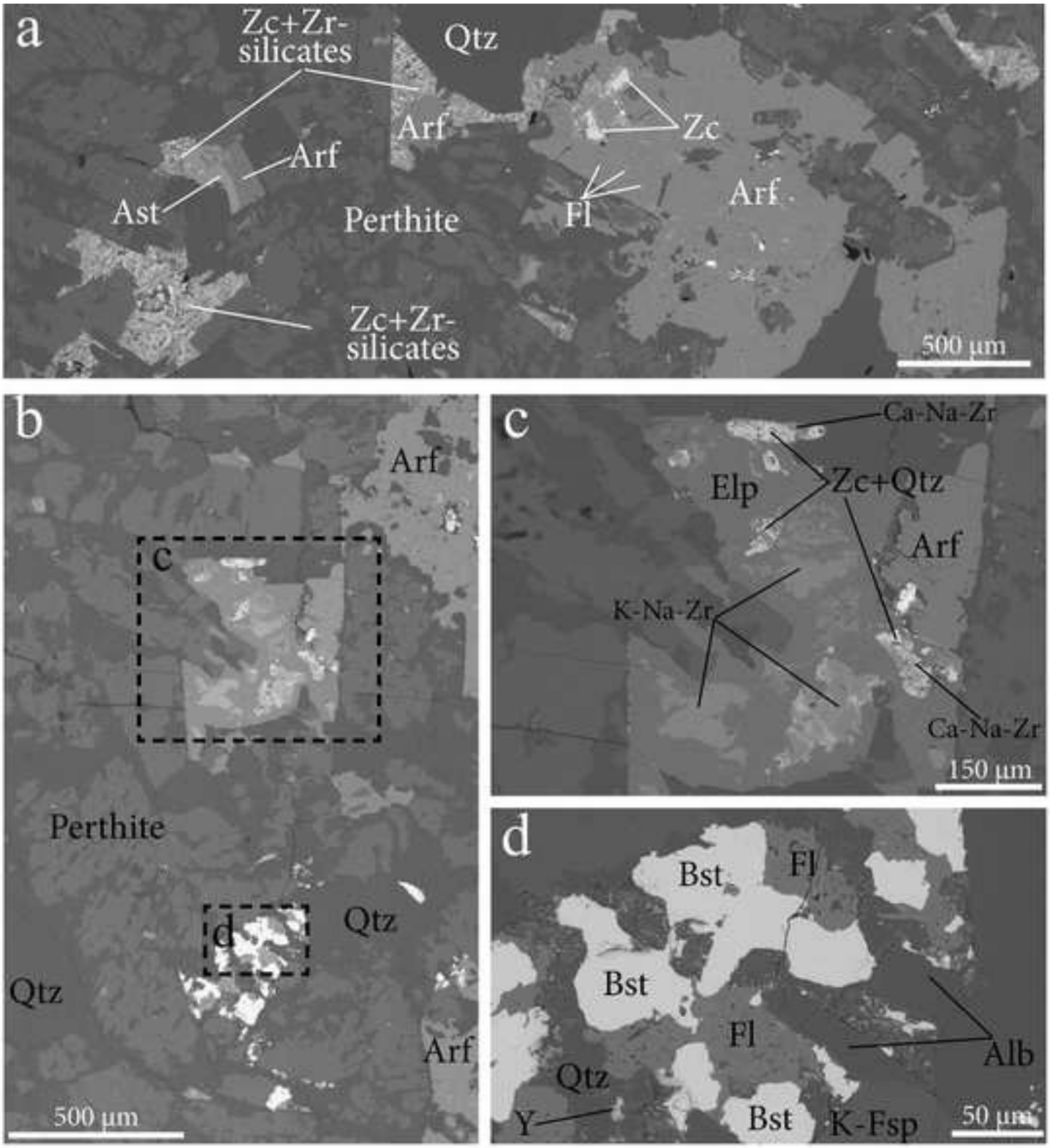

Vasyukova, O.V., Williams-Jones, A.E., 2016. The evolution of immiscible silicate and fluoride melts: implications for REE ore-genesis. Geochimica et Cosmochimica Acta 172, 205-224. DOI:10.1016/j.gca.2015.09.018

Figure 3

Click here to download high resolution image

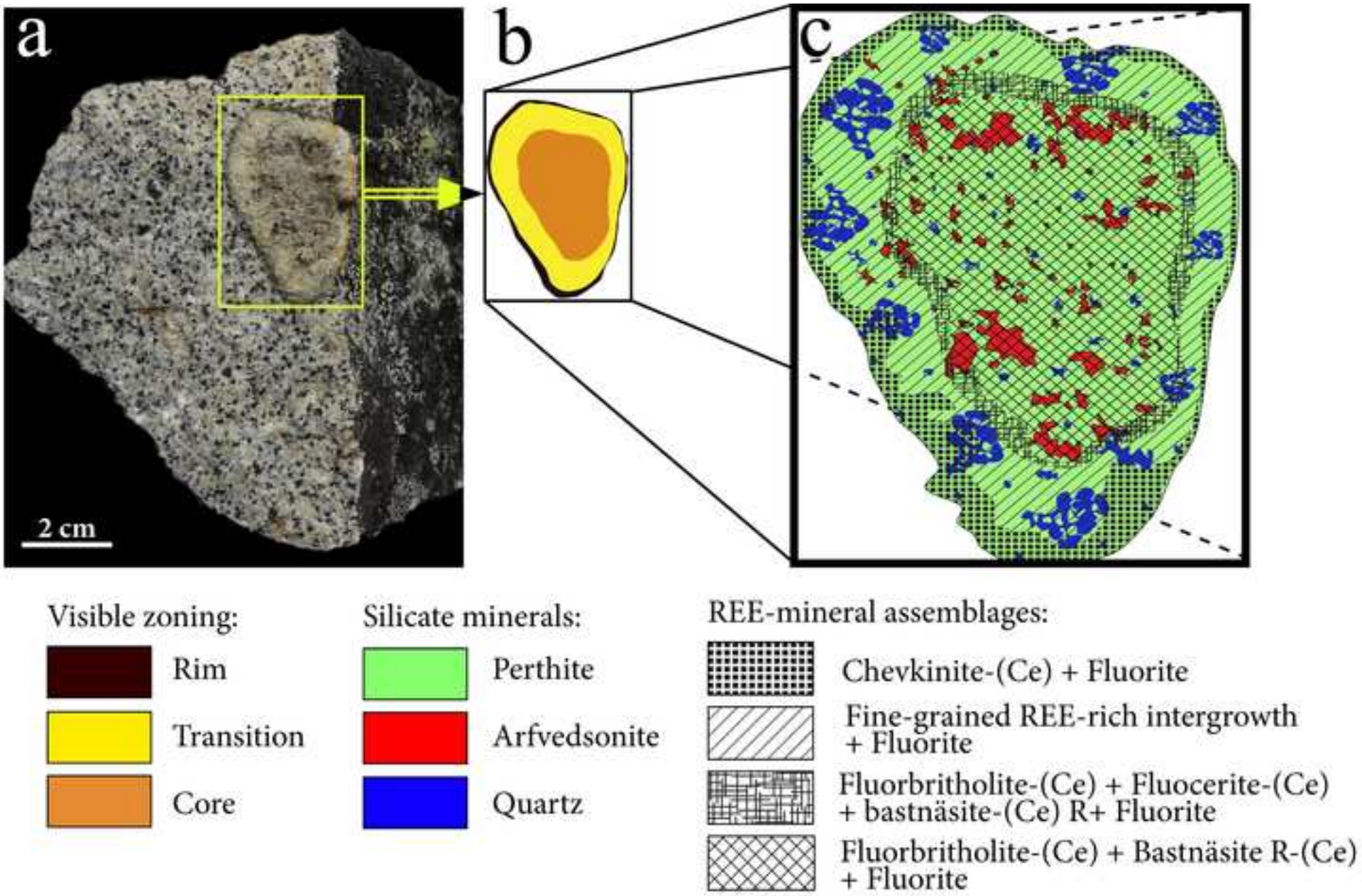

Vasyukova, O.V., Williams-Jones, A.E., 2016. The evolution of immiscible silicate and fluoride melts: implications for REE ore-genesis. Geochimica et Cosmochimica Acta 172, 205-224. DOI:10.1016/j.gca.2015.09.018

Figure 4

Click here to download high resolution image

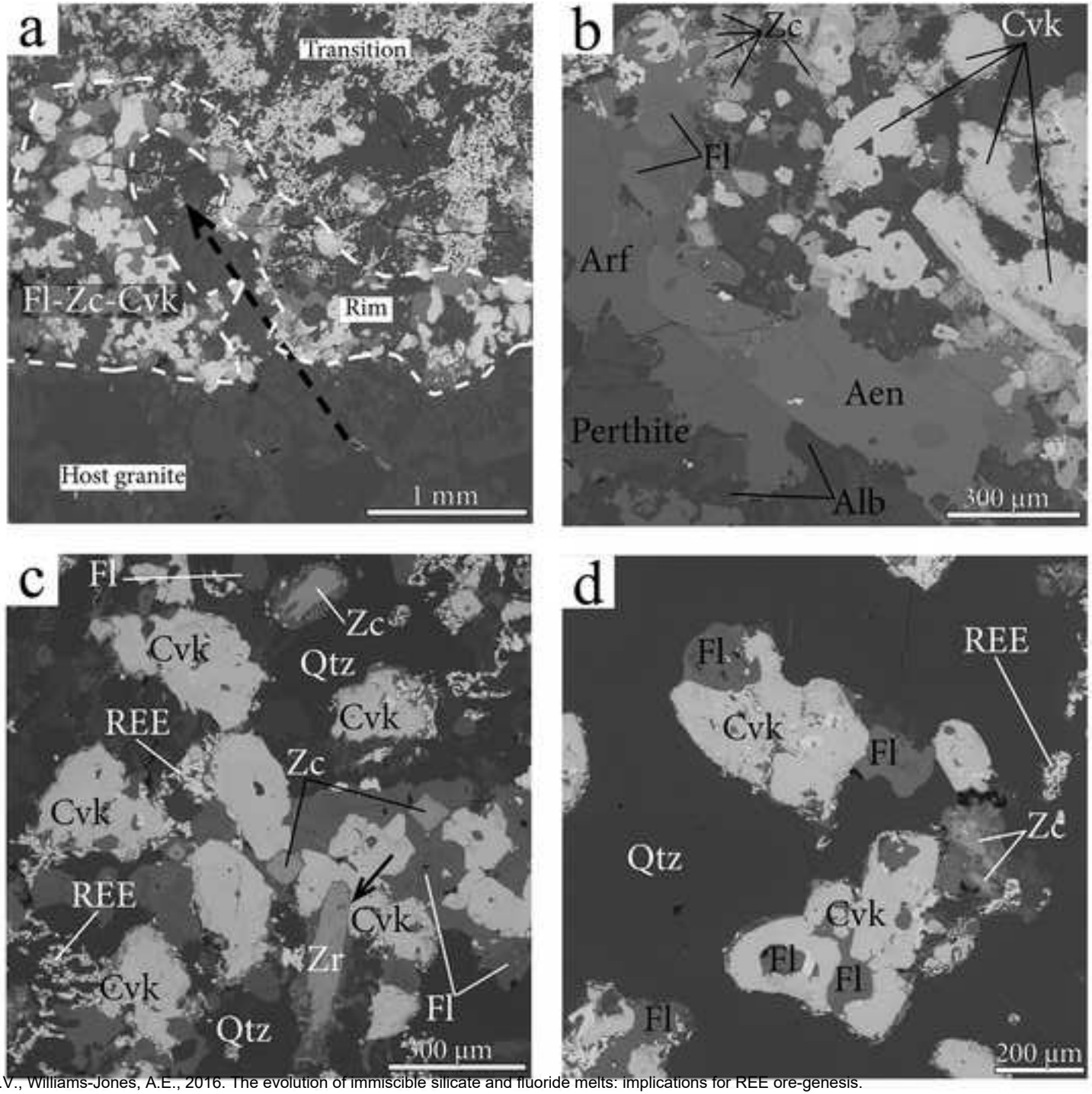

Vasyukova, O.V., Williams-Jones, A.E., 2016. The evolution of immiscible silicate and fluoride melts: implications for REE ore-genesis. Geochimica et Cosmochimica Acta 172, 205-224. DOI:10.1016/j.gca.2015.09.018

Figure 5

Click here to download high resolution image

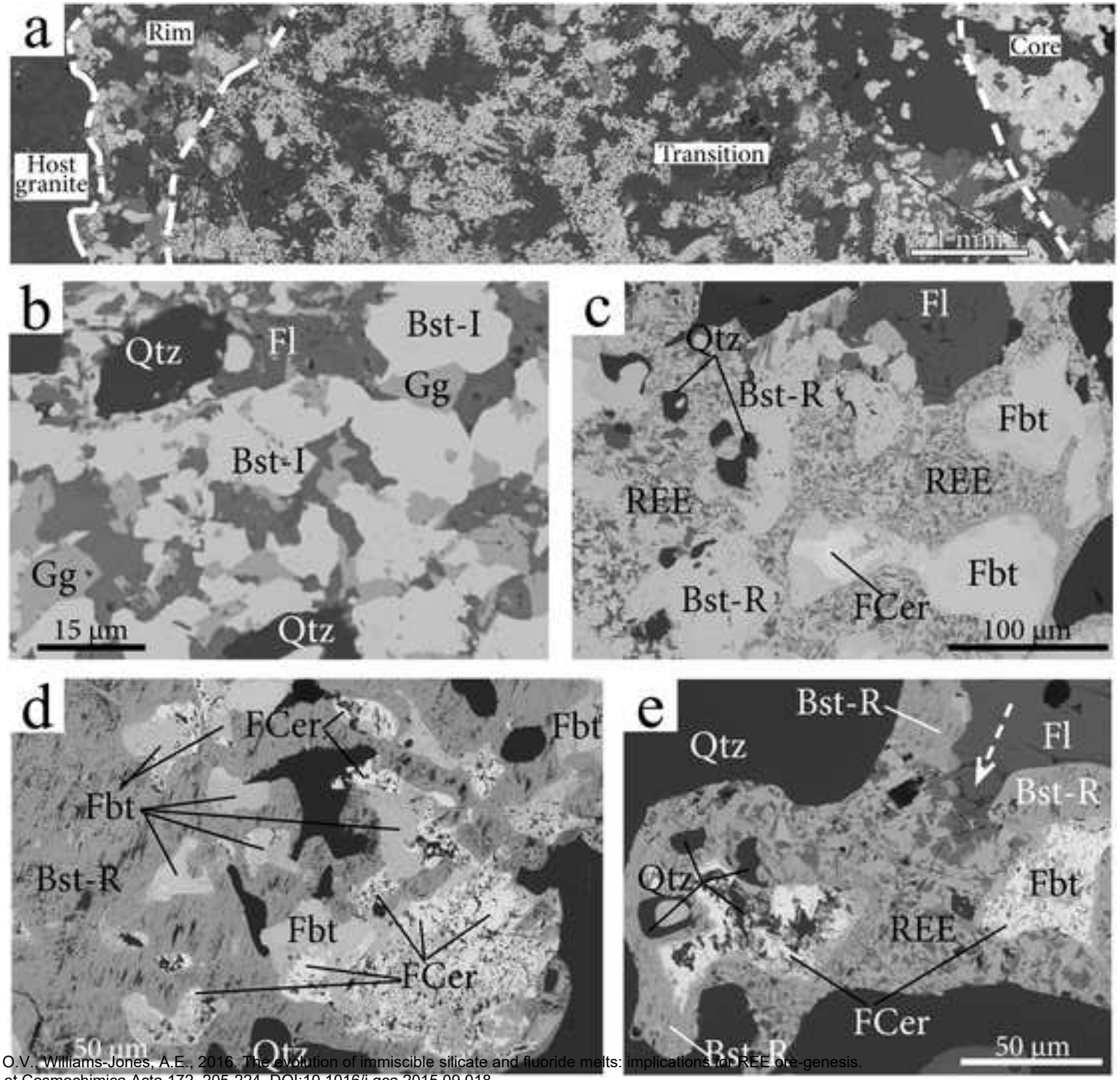

Vasyukova, O.V., Williams-Jones, A.E., 2016. The evolution of immiscible silicate and fluoride melts: implications for REE ore-genesis. Geochimica et Cosmochimica Acta 172, 205-224. DOI:10.1016/j.gca.2015.09.018

Figure 6

Click here to download high resolution image

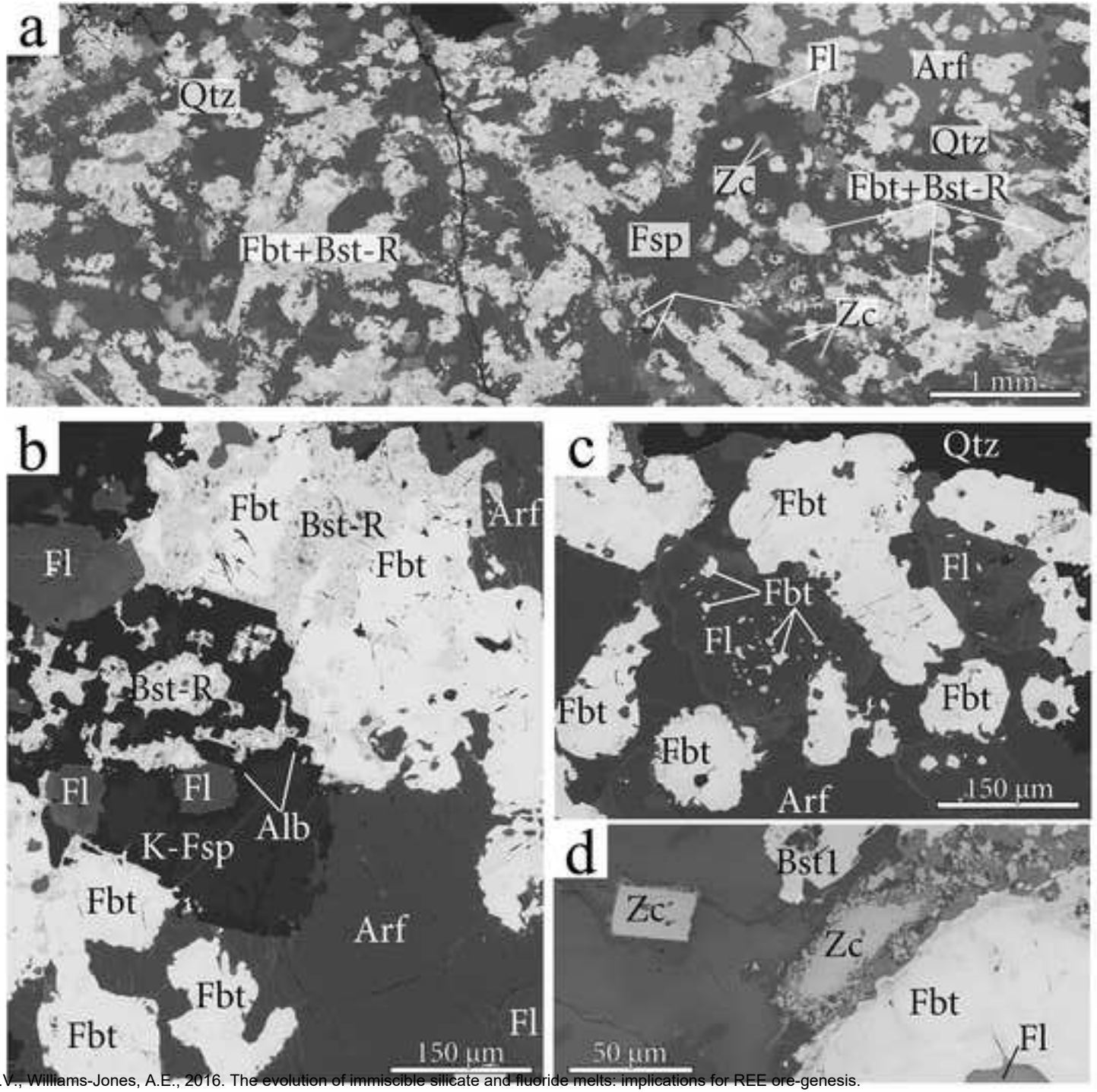

Vasyukova, O.V., Williams-Jones, A.E., 2016. The evolution of immiscible silicate and fluoride melts: implications for REE ore-genesis. Geochimica et Cosmochimica Acta 172, 205-224. DOI:10.1016/j.gca.2015.09.018

Figure 7

Click here to download high resolution image

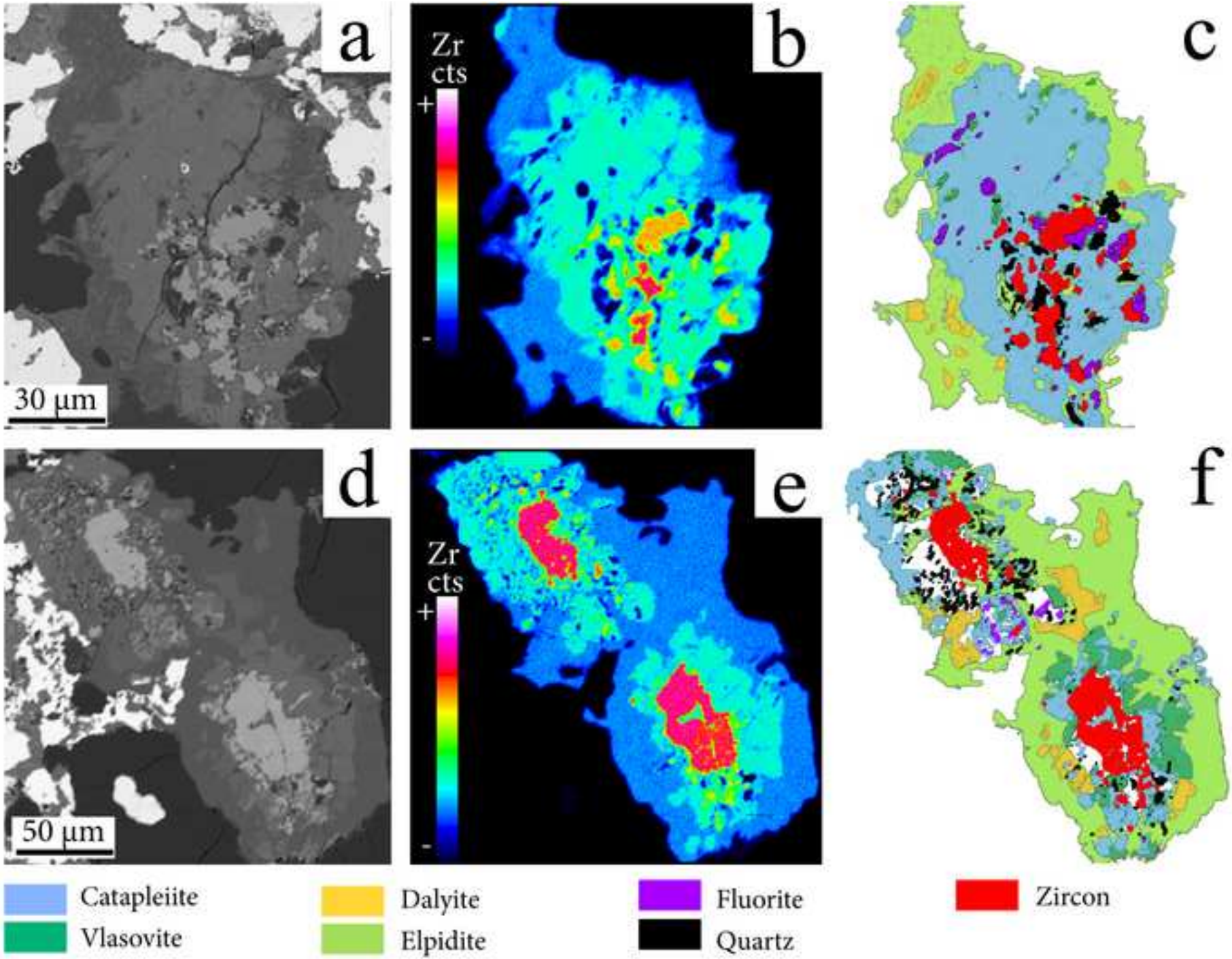

Vasyukova, O.V., Williams-Jones, A.E., 2016. The evolution of immiscible silicate and fluoride melts: implications for REE ore-genesis. Geochimica et Cosmochimica Acta 172, 205-224. DOI:10.1016/j.gca.2015.09.018

Figure 8

Click here to download high resolution image

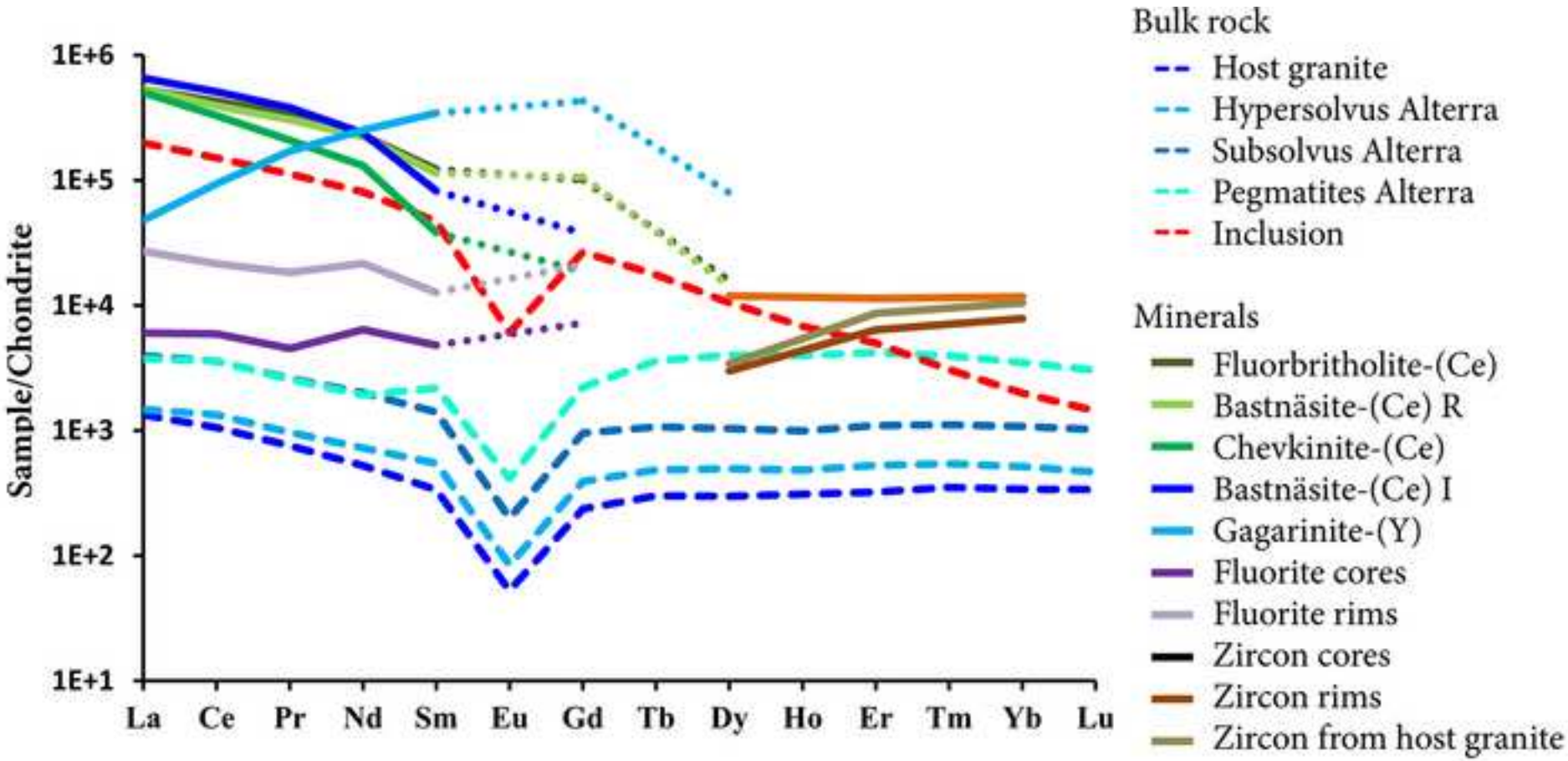

Vasyukova, O.V., Williams-Jones, A.E., 2016. The evolution of immiscible silicate and fluoride melts: implications for REE ore-genesis. Geochimica et Cosmochimica Acta 172, 205-224. DOI:10.1016/j.gca.2015.09.018

Figure 9

Click here to download high resolution image

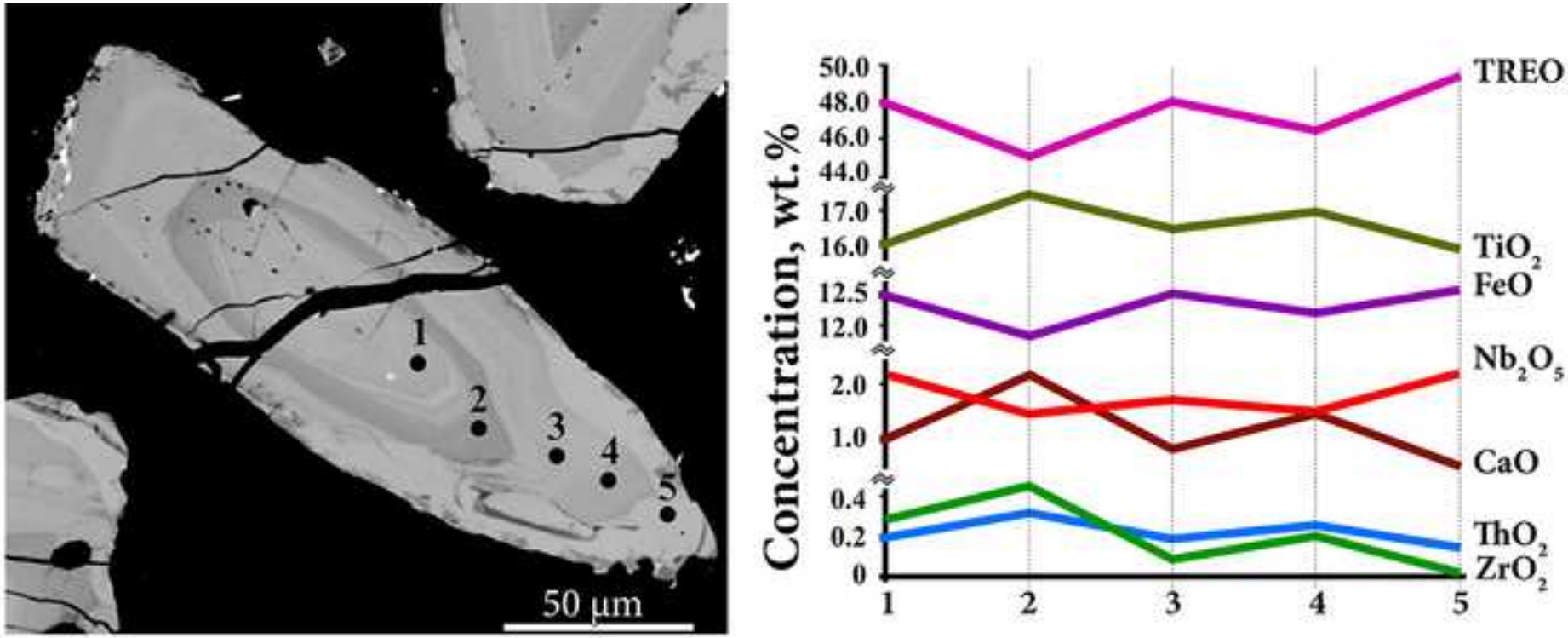

Vasyukova, O.V., Williams-Jones, A.E., 2016. The evolution of immiscible silicate and fluoride melts: implications for REE ore-genesis. Geochimica et Cosmochimica Acta 172, 205-224. DOI:10.1016/j.gca.2015.09.018

Figure 10

Click here to download high resolution image

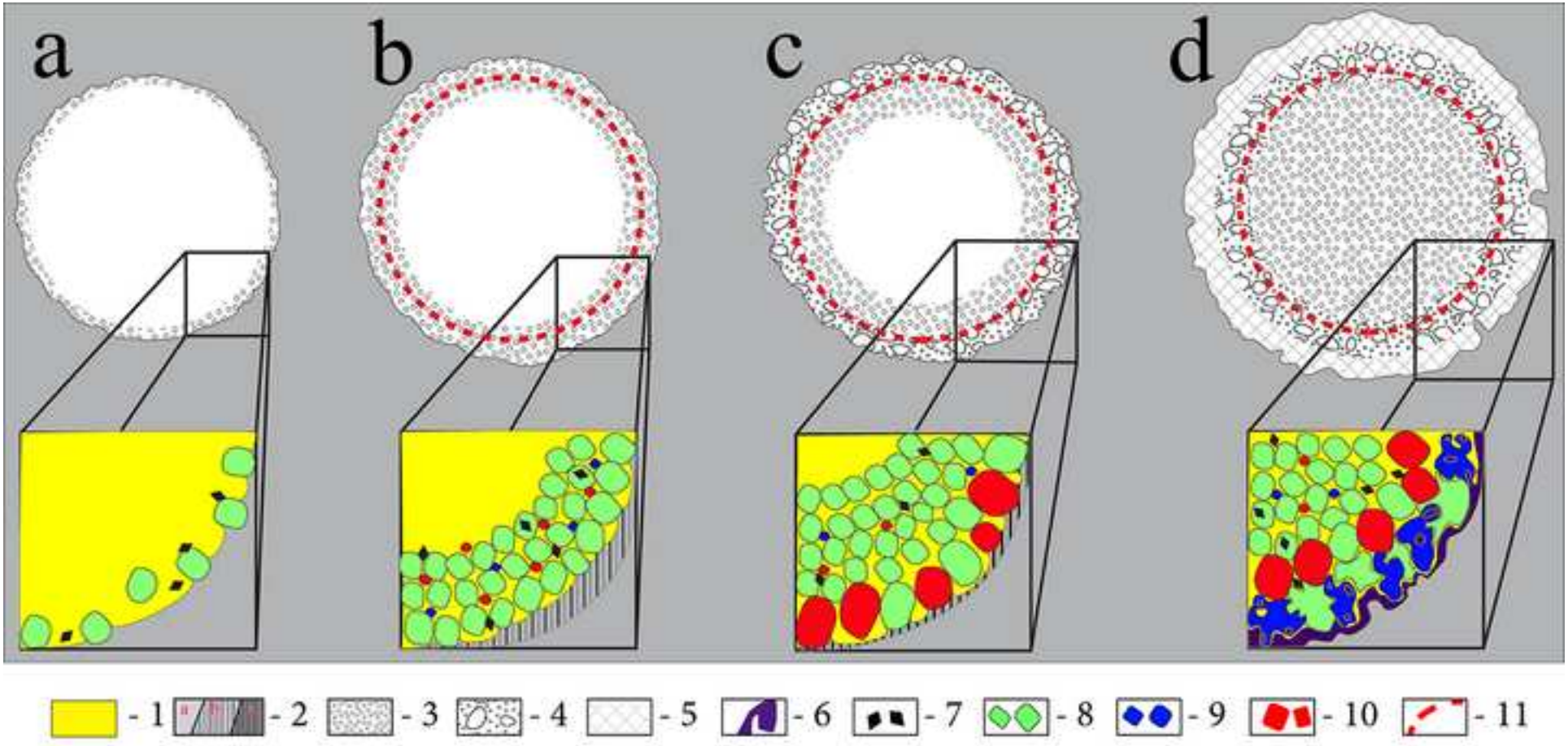

Vasyukova, O.V., Williams-Jones, A.E., 2016. The evolution of immiscible silicate and fluoride melts: implications for REE ore-genesis. Geochimica et Cosmochimica Acta 172, 205-224. DOI:10.1016/j.gca.2015.09.018